MEASUREMENTS OF SOLAR MAGNETIC FIELDS

Thesis by

Neil Rolfson Sheeley, Jr.

In Partial Fulfillment of the Requirements

For the Degree of

Doctor of Philosophy

California Institute of Technology

Pasadena, California

1965

(submitted May 5, 1965)

ACKNOWLEDGEMENTS

ABSTRACT

The photographic technique of Leighton (1) has been used to obtain high resolution measurements of photospheric magnetic fields with the following chief results:

1. "Source fluxes", Φ(defined as the average of the absolute values of the total fluxes of positive and negative polarity in a bipolar magnetic region on the day when this average is largest), of bipolar magnetic regions (BMRs) have been measured as a function of the "size", A_m, of the associated sunspot activity. [A_m is defined to be the area covered by all of the sunspots of a group (umbras plus penumbras of both leading and following parts) on the day when this area is largest.] The source fluxes were found to satisfy $\Phi = 1.2\ A_m$ within about $\pm\ 50\%$, where Φ is in "solar flux units" (1 SFU = 10^{21} maxwells) and A_m is in units of $10^{18}\ cm^2$. Within measurement accuracy there was no imbalance of flux of positive and negative magnetic polarity in the BMRs observed, provided that the photographically-obtained fluxes were supplemented by the fluxes in the umbras of sunspots, as calculated from Mount Wilson observations.

2. Two BMRs were traced for the first few months following their birth. The development of each was semi-quantitatively what one would expect if the random-walk (2) plus solar differential rotation were the only means of flux transport on the solar surface.

3. In quiet regions of the solar surface, magnetic flux is distributed in small bits and fragments, and in the quietest regions, in tiny points less than 3000 km in diameter. Measurements for eight small features yielded fluxes ranging from 0.05 SFU for the very small points to 0.4 SFU for typical network fragments. The corresponding magnetic fields ranged from 200 gauss for the points to 700 gauss for the network fragments, showing that magnetic fields of a few hundred gauss are not at all uncommon for small magnetic features.

4. Polar faculae curves (3) have been calibrated to give magnetic flux on the polar caps of the sun as a function of time during the period 1905-1964. The fluxes vary cyclicly with time approximately 90° out of phase with the variation of the sunspot number for the whole solar disk with time during this same period (provided the sunspot number is given a polarity corresponding to the magnetic polarity of the following sunspots of the relevant hemisphere). The maxima of the polar fluxes vary considerably from cycle to cycle (just as the maxima of the sunspot number vary considerably from cycle to cycle), maximum fluxes ranging from 6 SFU to 21 SFU with 12 SFU being a typical maximum polar flux during the 1905-1964 period.

The principal conclusion is that these measurements are consistent with the hypothesis that all of the magnetism on the sun's surface originates in BMRs, and that it is gradually spread about the surface by the random-walk (2, 4) and differential rotation, eventually causing the cancellation and reversal of the polar fields.

v

TABLE OF CONTENTS

I. Introduction

The findings of several investigators have provided the stimulus for the measurements described here. The following gives a brief account both of these findings and of the way in which they are related to our measurements.

Babcock's development of the solar magnetograph (5) led to the discovery of bipolar magnetic regions (BMRs) and of evidence for a main poloidal field of the sun (6). During their initial stages, BMRs are relatively small and have strong magnetic fields. Sunspot activity is common, and, except in the very smallest BMRs, sunspot groups of bipolar magnetic polarity generally appear. Hale's laws (7, 8) governing the magnetic polarity of sunspots also apply to the BMRs. As BMRs age, they expand and weaken, covering larger areas with smaller magnetic fields. They are detectable long after the sunspots have disappeared. In each hemisphere, a preponderance of the following parts of BMRs expand or drift toward the corresponding pole of the sun, while a preponderance of the leading parts of BMRs expand or drift toward the equator. The main poloidal field of the sun, observed during the last minimum of sunspot activity, weakened and underwent a reversal of magnetic polarity, first in the south and then in the north, about the time of the last maximum of sunspot activity. These results led Babcock (6) to hypothesize that in every cycle of sunspot activity the BMRs provide sources of magnetic flux, the leading parts of which move to the equator to neutralize their counterparts from the opposite hemisphere while the following parts move to the poles where they cancel the initial polar fields and then replace them with fields of opposite polarity.

Leighton's development of a method of photographically mapping solar velocity fields (9) and solar magnetic fields (1) led to the discovery of a system of non-stationary, large-scale convective cells on the surface of the sun (9), and to the observation (10) that in quiet regions of the sun magnetic fields are concentrated at the boundaries of these cells. This, in turn, led Leighton to propose a mechanism by which magnetic fields may be transported on the solar surface (2, 4). The mechanism is a random-walk associated with the non-stationary large-scale cellular convection. In particular, Leighton suggested that if sunspot groups are regarded as sources of magnetic flux, then, because the following parts of sunspot groups of each hemisphere tend to be closer to the corresponding pole than the leading parts (11), the net magnetic field transported to each pole would have the polarity of the following spots of the respective hemisphere. Since the polarity of the leading and following spots in each hemisphere reverses with each new cycle of sunspot activity (8), the random-walk provides a mechanism for the reversal of the polar fields in every cycle of sunspot activity.

Prior to this time Howard (12) had suggested comparing Mount Wilson spectroheliograms (SHGs) or direct photographs ("directs") with polar magnetograms to see if either the SHGs or "directs" could be used as a means of studying the polar fields. The author made a cursory study of the SHGs and magnetograms, concluding that, although chromospheric absorbing features (now believed to be spicules (13)) tend to block polar faculae from view, it might be possible to use either the H_α or K spectroheliograms as a means of studying the polar fields. However, the summer

observing season was approaching at Mount Wilson, and plans to study the polar fields were put aside for the apparently more fruitful study of chromospheric velocity fields. Soon after Leighton proposed the random-walk mechanism of flux transport (4), it became clear that studying polar faculae during the solar cycle would be a good way to test Leighton's ideas. The random-walk hypothesis predicted that the polar fields should reverse near the time of sunspot maximum in every sunspot cycle, and since there is a strong spatial correlation between the line-of-sight component of photospheric magnetic field and the intensity of solar faculae (1, 10), one would expect, a priori, that the number of polar faculae would vary with time in such a way as to attain a relative minimum about the time of sunspot maximum in every cycle. The numbers of north and south polar faculae visible on Mount Wilson "directs" were then counted for the period 1905-1964 with the result (3) that the number of polar faculae did indeed attain relative minima about the time of sunspot maximum in every cycle during the 1905-1964 period. (This result is included here in Appendix III.) This first success of the random-walk hypothesis provided the stimulus for measurements which might be used to test the mechanism further.

Part III (A) presents measurements of fluxes associated with sunspot groups as a function of sunspot group size. The method employs the photographic technique of Leighton, and thus has spatial resolution superior to that of other methods. This method has the further advantage that it is sensitive to strong fields, the calibration curve being linear from the threshold of approximately 50 gauss to approximately 1500 gauss. Both the method of obtaining these

measurements and the accuracy to which they have been obtained are described in Part II.

Once the coordinates and flux of a magnetic source have been measured, one might expect to test the random-walk hypothesis by observing the subsequent development of the BMR and comparing this with what one would expect from the combination of random-walk and solar differential rotation. Part III (B) describes the development of two sources over the period of a few rotations during the summer and autumn of 1964. This was an opportune time for such observations since there was very little other magnetic activity to interfere with the development of these BMRs.

In the process of obtaining the magnetic flux measurements, fluxes in relatively quiet regions were obtained. Small features having moderately large fluxes were found, suggesting the presence of strong small-scale magnetic fields. Magnetic field measurements of these small features then revealed field strengths a factor of ten larger than have heretofore been reported (10) for small features in quiet regions of the sun. Because of the superior spatial resolution and sensitivity to strong fields, Leighton's photographic technique is especially good for studying these small-scale magnetic fields. These measurements are described in Part III (C).

Finally, a method of calibrating the number of polar faculae in terms of magnetic flux normal to the solar surface has been found, and is described in Part III (D).

In Part IV the results are summarized and some possible interpretations offered.

II. The Method and Accuracy of Magnetic Flux Measurement

This thesis is concerned primarily with measurements of solar magnetic flux. The flux measurements described here were derived from Zeeman photographs (1) obtained by the author at the 60-foot tower on Mount Wilson during the summer and autumn of 1963 and 1964. The method and accuracy of the magnetic flux measurement is described in four parts: The first part describes the method of obtaining the Zeeman photos. The second part describes the way in which the magnetic fluxes were derived from these photos. The third part gives an account of the sensitivity of the method to fluxes in sunspots. The fourth part describes some sources of error and attempts to summarize the accuracy of the measurements.

A. The Method of Obtaining Zeeman Photographs

The method employed was developed by Leighton and has been described in detail by him (1). Therefore, only the basic procedure will be described here.

The spectroheliograph at the 60-foot tower was fitted with an optical beam splitter and fixed analyzers for right- and left-hand circularly polarized light. With a solar image of approximately 17 cm in diameter, two simultaneous spectroheliograms of the region of interest were obtained at a wavelength corresponding to a steep part of the Ca $\lambda6103$ line profile. The entrance and exit slits of the spectroheliograph were 0.05 mm and 0.06 mm respectively, and the exit slit was positioned approximately 0.05 mm to the violet of the line core. The spectrum was viewed in the second order with a dispersion of 1.44 $\frac{A}{mm}$. After such a pair of spectroheliograms

had been obtained, the polarization sense of the analyzer was
reversed, the photographic plate position was shifted, and another
pair of simultaneous spectroheliograms was taken on the same
photographic plate. Following this, the plate position was shifted
again and an expanded line profile of the $\lambda 6103$ line was made for
calibration purposes. By image superposition and a photographic
subtraction process a picture was obtained in which lighter-than-
average features represented areas of one magnetic polarity and
darker-than-average features represented areas of the other
magnetic polarity. Such a picture is called a Zeeman photograph,
or Z-photo as we shall now refer to it. For each Z-photo a cali-
bration curve was obtained by making a microphotometer tracing
of the expanded line profile on the original plate and plotting log T
(the logarithm of the transmission) versus wavelength. (The micro-
photometer was equipped with an analog computer which allowed
operation in such a way that the output of the microphotometer read
log T directly rather than just transmission. Since approximately
forty such profiles were traced, this saved considerable effort.)
Differences in log T on the Z-photo were then related to differences
in log T on the calibration curve by a factor of four due to a four-
fold enhancement of contrast in the image superposition and photo-
graphic subtraction process. Figure 1 shows a typical calibration
curve. Note that the exit slit of the spectroheliograph was positioned
relative to the line profile such that changes in $\log_{10} T_{orig}(\lambda)$ are
linear for changes in $\Delta\lambda$ up to $\pm$ 0.07 A. This corresponds to mag-
netic fields up to $\pm$ 2000 gauss.

Figure 1

Calibration curve for the Z-photo of September 9, 1964 in which $\log_{10} T_{orig}(\lambda)$ is plotted versus λ. Negative values of λ refer to the violet wing of the line and positive values refer to the red wing. The sharp peaks superimposed on the profile are fiducial marks used to calibrate the wavelength scale.

Figure 1
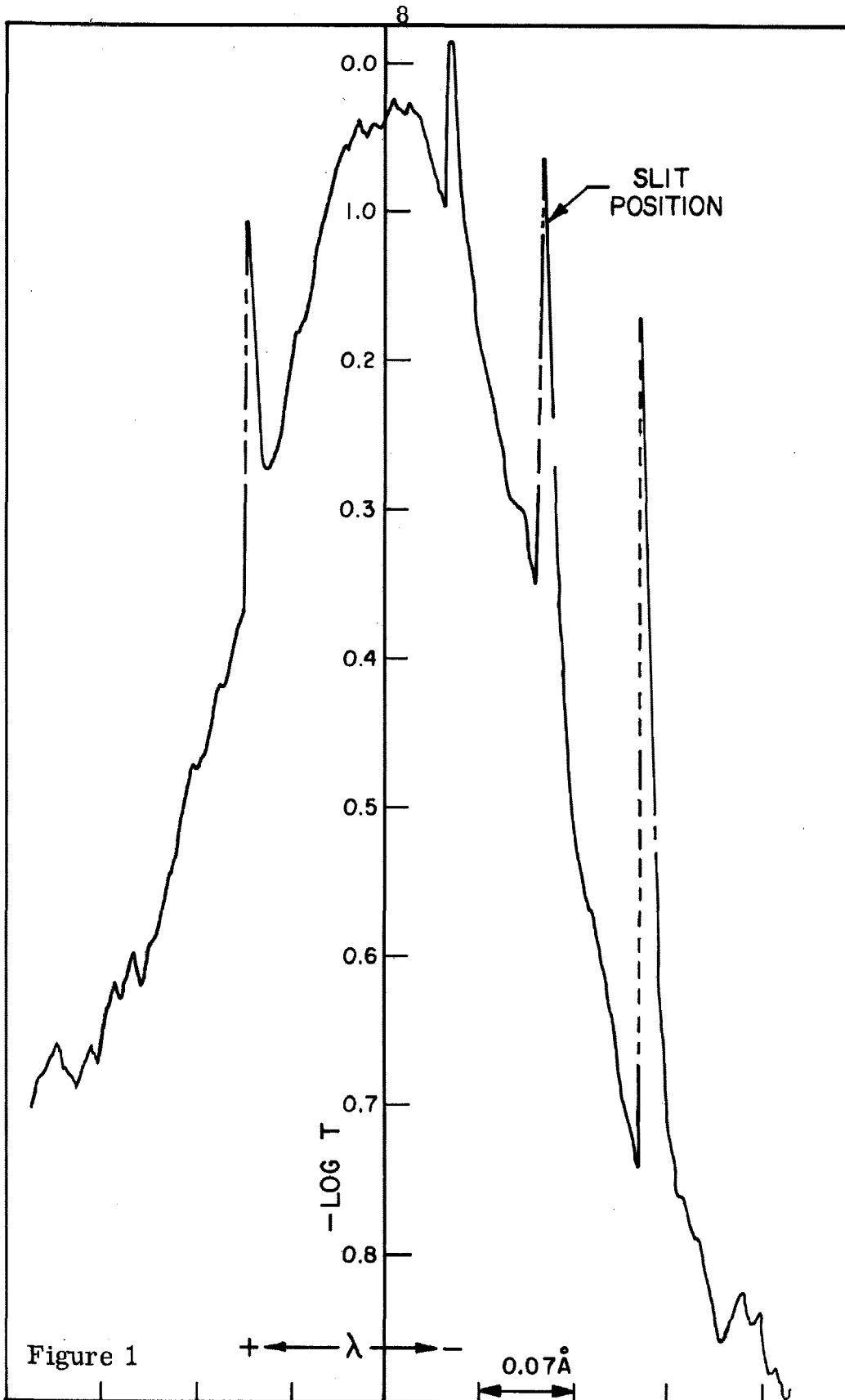
B. The Method of Obtaining Magnetic Fluxes from Z-photos

The method described here is not the only way to derive magnetic fluxes from Z-photos. This section tells why this particular method was selected and then describes the method in detail.

Perhaps the most straightforward method of obtaining magnetic flux from a Z-photo is by directly integrating the magnetic field over the area of interest. First one could make a series of fine scan tracings of log T over the region of interest. Next, using the calibration curve for this Z-photo, the series of tracings of log T could be converted into a series of tracings of magnetic field strength. Finally, by adding together the areas between the magnetic field tracings and a suitable zero-field level and multiplying this sum by the known scanning width of the tracings, one would obtain the flux across the area of interest. This method was tried and found to have some severe disadvantages. First, the procedure was very time-consuming and laborious. A few days were required to obtain the flux in a typical BMR. The long, tedious nature of the method gave rise to occasional mistakes. This, together with the lack of a quick and simple method of checking the measurements, thus made the results somewhat dubious. Second, this procedure did not make use of the advantages of a two-dimensional picture of the magnetic field pattern. The two-dimensional field pattern would have aided considerably in distinguishing variations in transmission due to magnetic fields from variations due to other causes. Third, this procedure of finding the flux in a BMR did not show how the flux was distributed throughout the BMR. The

distribution was of interest because much of the flux was concentrated generally in small features scattered throughout the BMR.

Because of the severe disadvantages of the method described above, a more practical way of obtaining magnetic fluxes from Z-photos was sought and found. Basically, this method employs a wide-aperture photometer to photoelectrically integrate magnetic fields in selected regions of Z-photos. The method has the advantages of speed, simplicity, and two-dimensionality. One can select a region or feature on a Z-photo, and in a few minutes obtain the magnetic flux in this region or feature by means of four simple transmission measurements. No tracings on chart paper and no tedious computations are necessary. The result is a Z-photo in which each magnetic feature is labeled with its flux. The method has three disadvantages. First, the bias of the observer enters in his visual selection of regions or features that contribute flux to a BMR. This is especially important when there are many features with fluxes near the threshold of measurement, such as in an old BMR, so that the neglect of several such features would cause the total measured fluxes to be too low. Second, instead of one Z-photo for each region of interest, a pair of Z-photos having reciprocal transmissions is needed. This increases the accuracy of the measurements, as will be described below. The requirement of a pair of Z-photos is not a major disadvantage since such a pair can be obtained almost as easily as a single photograph. Third, calibration of the flux is obtained indirectly from the calibration curve rather than directly as will be described below. This may reduce the accuracy of the measurements slightly, but the advantage of immediate, easily-verifiable fluxes for features chosen from

Z-photos far outweighs slight inaccuracies introduced by this method. The method will now be considered in detail.

It was found that Leighton's autocorrelation machine (9) could be used to measure relative transmissions on Z-photos simply and conveniently. First we shall describe the way in which magnetic fluxes can be obtained from such transmission measurements, and then we shall give an account of the measuring procedure itself.

One can show (10) that under certain conditions the transmission of a Z-photo is given by:

$$(1) \qquad T/T_0 = \left(\frac{1 + \delta}{1 - \delta}\right)^{2\gamma_M},$$

where T and T_0 are the respective transmissions in field and non-field regions, γ_M is the photographic gamma of the original plate (typically $\gamma_M \sim 3.0$), and δ is proportional to the magnetic field as will be seen in equations (2) and (3) below. The conditions are:

1) that the exposure of the original photographic plate lies on the linear portion of the characteristic curve of the original plate,

2) that the magnetic fields encountered are not so strong that they shift the exposure off the linear portion of the characteristic curve,

3) that unity gamma is achieved in each stage of reduction from the original plate to the final Z-photo.

δ is given by:

$$(2) \qquad \delta = \Delta\lambda\cos\gamma \left\{\frac{-I_0'(\lambda)}{I_0(\lambda)}\right\},$$

where $I_0(\lambda)$ is the intensity of radiation from field-free regions of the sun (i. e. the intensity of the π-component of radiation), and is evaluated at the wavelength at which the spectroheliograms were taken. γ is the angle between the magnetic field direction and the line-of-sight. $\Delta\lambda$ is the Zeeman splitting, and for $\lambda6103$ is given by:

$$(3) \quad \Delta\lambda = 3.47 \times 10^{-5} \, B \; A/gauss,$$

where B is the magnitude of the magnetic field. A calibrated step-wedge permitted the characteristic curve of the original plate to be drawn, and using this together with the expanded line profile, one obtains typically $3.0A^{-1}$ for $\dfrac{I_0{}'(\lambda)}{I_0(\lambda)}$. Using equation (3) we obtain $\Delta\lambda \approx 0.035A$ for a magnetic field of 1000 gauss, and if this field is directed along the line-of-sight, equation (2) yields
$\delta \sim 0.035 \times 1 \times 3.0 \sim 0.1.$

Next, consider a power series expansion of the expression for the transmission on a Z-photo (equation (1)):

$$(4) \quad T/T_0 = 1 + 4\gamma_M\delta + \ldots \; .$$

The first-order term, $4\gamma_M\delta$, is proportional to the line-of-sight component of magnetic field and will be used as an "intermediate" between transmission measurements and the magnetic field. That is, we shall obtain $4\gamma_M\delta$ from transmission measurements, and then obtain the line-of-sight field from $4\gamma_M\delta$. Making a linear approximation to the characteristic curve of the original plate, one can easily show from the definitions above:

$$(5) \quad 4\gamma_M\delta = 3.20 \times 10^{-4} \ B_{\|} \ \left\{ \frac{d\log_{10}T_{orig}(\lambda)}{d\lambda} \right\} \ \text{A/gauss},$$

where $B_{\|} = B\cos\gamma$, and $T_{orig}(\lambda)$ is the transmission of the expanded line profile on the original plate as a function of wavelength. Thus, $\frac{d\log_{10}T_{orig}(\lambda)}{d\lambda}$ is the slope of the calibration curve at the wavelength at which the spectroheliograms were taken. Hence, $B_{\|}$ can be determined from $4\gamma_M\delta$ using the calibration curve.

First consider weak magnetic fields. If $B_{\|} \ll 1000$ gauss, then $\delta \ll 0.1$, and only terms up to first-order need be retained in the expansion of T/T_0. In this case, $4\gamma_M\delta = \frac{\Delta T}{T_0}$ and the magnetic field can be obtained from a measurement of $\frac{\Delta T}{T_0}$.

Next consider fields sufficiently strong that one does not have $B_{\|} \ll 1000$ gauss. Suppose, for example, that $B_{\|} \approx 1000$ gauss so that $\delta \approx 0.1$. Now, terms of order greater than first-order must be retained in the expansion of T/T_0 (equation (4)) to accurately represent T/T_0 (equation (1)). For a typical $\gamma_M \approx 3.0$, $\frac{\Delta T}{T_0} = (\frac{1.1}{0.9})^6 - 1 = 2.3$, whereas $4\gamma_M\delta = 4 \times 3.0 \times 0.1 = 1.2$. Clearly, $4\gamma_M\delta \neq \frac{\Delta T}{T_0}$. However, $4\gamma_M\delta$ can be obtained from both $\frac{\Delta T}{T_0}$ and one additional measurement of relative transmission:

Suppose that, in addition to the Z-photo having the transmission T given by equation (1), one had a second Z-photo having transmission T, reciprocal to that of the first photograph given by:

$$(6) \quad T/T_1 = \left(\frac{1-\delta}{1+\delta}\right)^{2\gamma_M},$$

where T_1 is the background transmission of the second Z-photo. Using $\gamma_M \approx 3.0$ and $\delta \approx 0.1$ one finds $\frac{\Delta T}{T_1} = -0.7$ for the second photograph. The geometric mean of $\frac{\Delta T}{T_0} = 2.3$ and $|\frac{\Delta T}{T_1}| = 0.7$ is $(\frac{\Delta T}{T})_{GM} = \sqrt{2.3 \times 0.7} = 1.3$, differing by less than 10% from $4\gamma_M\delta = 1.2$. It is shown more generally in Appendix I that, if $(\frac{\Delta T}{T})_+$ and $(\frac{\Delta T}{T})_-$ are the relative transmissions at the same solar position on each of the two photographs of such a pair of Z-photos, then their geometric mean:

$$(7) \quad (\frac{\Delta T}{T})_{GM} = \sqrt{(\frac{\Delta T}{T})_+ \times |(\frac{\Delta T}{T})_-|}$$

approximates $4\gamma_M\delta$ accurately for fields up to 1000 gauss. Thus the measurements of $(\frac{\Delta T}{T})_+$ and $(\frac{\Delta T}{T})_-$ allow the determination of $4\gamma_M\delta$ from which one can find $B_{||}$ using the calibration curve obtained from the expanded line profile.

Next, using our method of obtaining weak magnetic fields from transmission measurements, we shall synthesize a method of obtaining the magnetic flux of weak fields from transmission measurements. From the expression for the transmission $T(x,y)$ at a point (x,y), we shall form the quantities C and C_0 which represent the transmissions through an area A_0:

$$(8a) \quad C = \int_{A_0} T(x,y)\, dA$$

$$(8b) \quad C_0 = \int_{A_0} T_0\, dA\,.$$

We then define the quantity R by

$$(9) \quad R = \frac{C - C_0}{C_0} ,$$

and show that $A_0 R$ is proportional to the magnetic flux through the area A_0: From these definitions, one obtains directly:

$$(10) \quad A_0 R = \int_{A_0} \left(\frac{\Delta T}{T_0} \right) dA.$$

Now, for small fields, $\frac{\Delta T}{T_0} = 4\gamma_M \delta$, and we already know that $4\gamma_M \delta$ is proportional to $B_{||}$ (equation (5)). Hence

$$(11) \quad A_0 R = 3.20 \times 10^{-4} \left\{ \frac{d \log_{10} T_{orig}(\lambda)}{d\lambda} \right\} \Phi_{||} \quad A/gauss,$$

where $\Phi_{||} = \int_{A_0} B_{||} \, dA.$ Thus $\Phi_{||}$ can be obtained from two

measurements of transmission integrated over a known area
together with the calibration curve obtained from the expanded
line profile on the original plate.

Finally, in a manner similar to the one employed to generalize
the method of measuring weak fields to include strong fields, we
shall generalize this method of measuring flux to include flux from
strong fields. As before, one considers a geometric mean of two
quantities obtained from corresponding features on each of the two
photographs of a pair of Z-photos. In Appendix II, it is shown that

if A_0R^+ and A_0R^- are the quantities corresponding to the integrals of $(\frac{\Delta T}{T})_+$ and $(\frac{\Delta T}{T})_-$ respectively (equation (10)), then the geometric mean:

$$(12) \quad (A_0R)_{GM} = \sqrt{(A_0R^+) \times |A_0R^-|}$$

approximates $\int_{A_0} (4\gamma_M{}^\delta)dA$ accurately for fields up to 1000 gauss, and with a tolerable error for fields several hundred gauss larger. Thus, we can extend the relation between A_0R and $\Phi_{||}$ (equation (11)) to include strong fields:

$$(13) \quad (A_0R)_{GM} = 3.20 \times 10^{-4} \left\{ \frac{d \log_{10} T_{orig}{}^{(\lambda)}}{d\lambda} \right\} \Phi_{||} \text{ A/gauss.}$$

The flux measurements described in this thesis were obtained from measurements of $(A_0R)_{GM}$ using equation (13).

Having described the way in which magnetic flux can be obtained from transmission measurements, we shall now give an account of the measuring procedure itself. The autocorrelation machine described by Leighton, Noyes, Simon (9) was modified for use as a wide-aperture photometer. One of the two photographs of a pair of Z-photos was placed between the condensing lenses of the optical system. (We shall sometimes refer to these photographs as Zeeman plates instead of Zeeman photographs since they were on 4"x 5" glass photographic plates.) A solar region was selected and a mask with an aperture of known area was placed over the plate such that the region of interest was covered by the aperture. Parallel light from the first condensing lens passed through the aperture, and was

concentrated on the photocathode of a 931A photomultiplier tube by the second lens. A signal proportional to $C = \int_{A_0} T(x, y)\, dA$ was indicated on the dial of a photoelectric photometer. This signal was then recorded. Next the aperture was moved to a neighboring zero-field region of the plate and a signal proportional to $C_0 = \int_{A_0} T_0\, dA$ obtained and recorded. The quantity $R = \dfrac{C - C_0}{C_0}$ was calculated from these two readings and then multiplied by the aperture area A_0 to give $A_0 R^+$. Next, the plate was removed and the plate having transmission reciprocal to this first plate was inserted. Using the same solar region as before, two signals were recorded and a corresponding quantity R^- was calculated. Then R^- was multiplied by A_0 to give $A_0 R^-$. The geometric mean, $(A_0 R)_{GM}$, of $A_0 R^+$ and $-A_0 R^-$ was then calculated, and the flux was obtained using relation (13) above with the calibration curve for this particular pair of Z-photos.

The transmission of the zero-field region was always measured near the field region of interest for two reasons. First, large variations in the zero-field transmission across the plate could be avoided. Second, smaller variations in the intensity of light incident on different regions of the photographic plate could be avoided. This was possible because the regions of interest were small compared to the aperture of the first condensing lens.

For a given field region, the quantity $A_0 R$ was independent of the size of the aperture A_0 provided the aperture always covered the same flux, and provided the aperture was not so large that the variations in the zero-field transmission became a problem. In practice the aperture was chosen just large enough to cover the

region of interest and not much larger. The apertures were square
and ranged in size from 2mm x 2mm to 5mm x 5mm. The minimum
flux measureable corresponded to $RA_0 \approx 0.04 \times 4(mm)^2 = 0.16 \, (mm)^2$
which typically gave $0.16 \, (mm)^2 \times 0.5 \dfrac{SFU}{(mm)^2} = 0.08 \, SFU$. (We adopt
10^{21} maxwells as the unit of solar magnetic flux (SFU) throughout
this thesis.) Actually, for fluxes this small, the accuracy was not
very good, so that one could only estimate a threshold between
0.05 SFU and 0.1 SFU. The values of $\dfrac{d\log_{10} T_{orig}(\lambda)}{d\lambda}$ obtained
from the calibration curves varied considerably from plate to plate,
ranging from $3.0 \, A^{-1}$ to $8.0 \, A^{-1}$. Typically,

$$(14a) \quad \Phi_{||} = 0.5 \dfrac{SFU}{(mm)^2} \times (A_0 R)_{GM}$$

$$(14b) \quad B_{||} = 780 \text{ gauss} \times \left(\dfrac{\Delta T}{T}\right)_{GM}.$$

C. Sensitivity of the Method to Fluxes in Sunspots

The sensitivity of the measuring method described here
depends on two factors:

1) the photographic contrast, γ_M

2) the spectral sensitivity, $\dfrac{I_0'(\lambda)}{I_0(\lambda)}$.

γ_M is the slope of the characteristic curve of the original plate
corresponding to the exposure of the solar feature of interest.
$I_0(\lambda)$ is the intensity of the π-component of radiation at the wavelength
λ at which the spectroheliograms were taken. Near the disk center,

where limb darkening is negligible, most solar features have roughly the same exposure so that γ_M and $\dfrac{I_0{}'(\lambda)}{I_0(\lambda)}$ do not vary appreciably from the average. This is shown by the general lack of contrast on spectroheliograms taken at various positions on the $\lambda 6103$ line profile. Sunspots are notable exceptions. Thus, except for sunspots, a combined sensitivity may be obtained from the expanded line profile of the average spectrum of the solar disk

using the relation $\gamma_M \dfrac{I_0{}'(\lambda)}{I_0(\lambda)} = -2.30 \left\{ \dfrac{d\log_{10} T_{orig}(\lambda)}{d\lambda} \right\}$, where

$T_{orig}(\lambda)$ is the transmission of the expanded line profile as a function

of wavelength. There is a variation in $\left\{ \dfrac{d\log_{10} T_{orig}(\lambda)}{d\lambda} \right\}$ from

disk center to limb, the value decreasing by approximately 25% toward the limb. However, this variation is automatically corrected

by measuring $\left\{ \dfrac{d\log_{10} T_{orig}(\lambda)}{d\lambda} \right\}$ at the disk position where the

magnetic field of interest is located. Figure 2(a) and Figure 2(b)

show measurements of $\left\{ \dfrac{d\log_{10} T_{orig}(\lambda)}{d\lambda} \right\}$ at various positions from

center to limb for the plate of September 13, 1964.

Next, let us consider sunspots. Since both the spectra and intensities of sunspots differ considerably from the spectrum and intensity of the average solar disk, one cannot in general expect the expanded line profile of the average solar disk to yield a true measure of the sensitivity toward fields in sunspots. Therefore, let us consider the photographic contrast, γ_M, and the spectral sensitivity, $\dfrac{I_0{}'(\lambda)}{I_0(\lambda)}$, separately.

Figure 2

(a)   Calibration curves obtained at three different distances
from the disk center for the Z-photo of September 13, 1964.
θ refers to the approximate longitude of the position for
which the curve was obtained.

(b)   The sensitivity $M(M = \frac{d}{d\lambda} \log_{10} T_{orig}(\lambda))$ as a function of
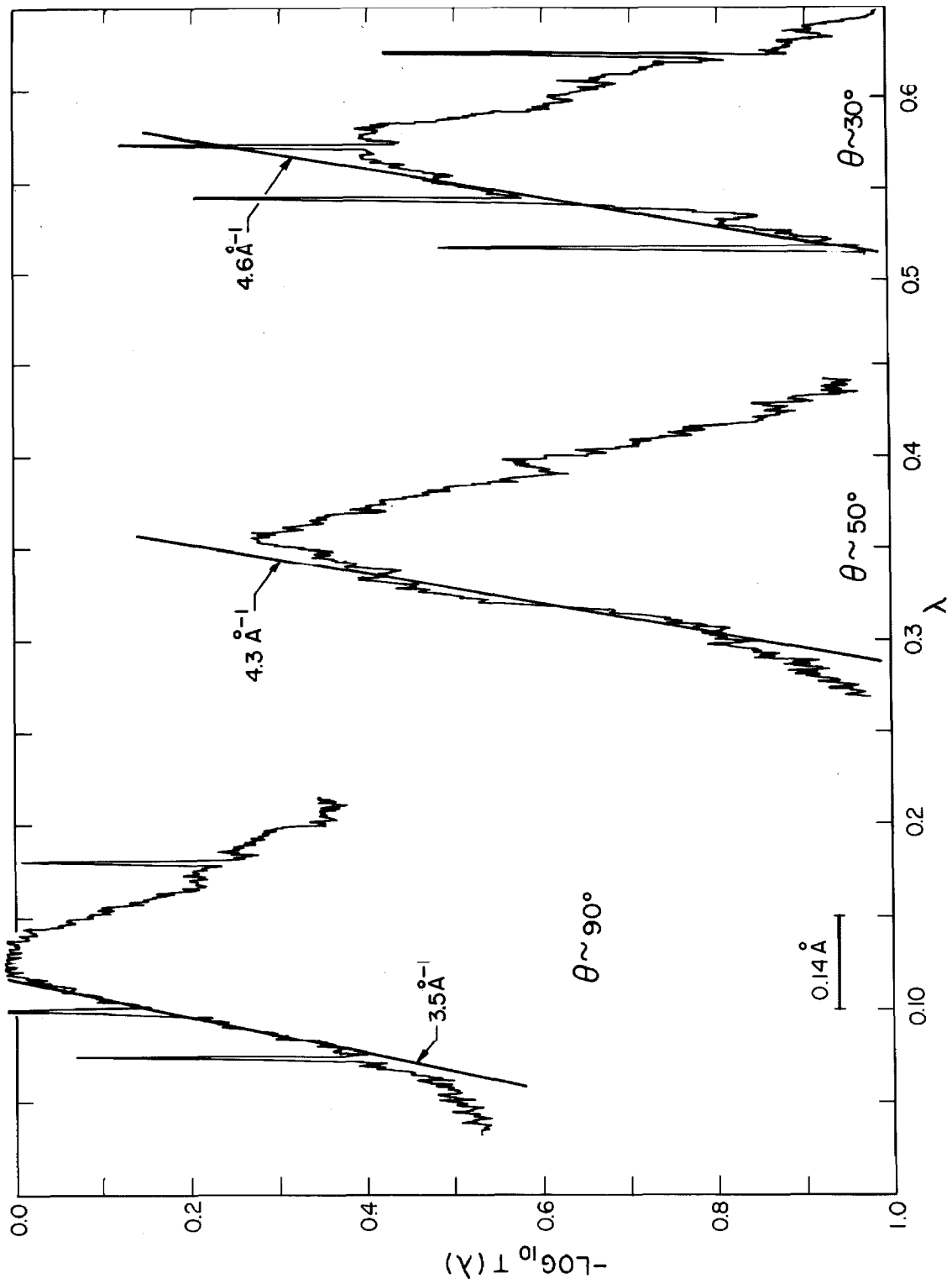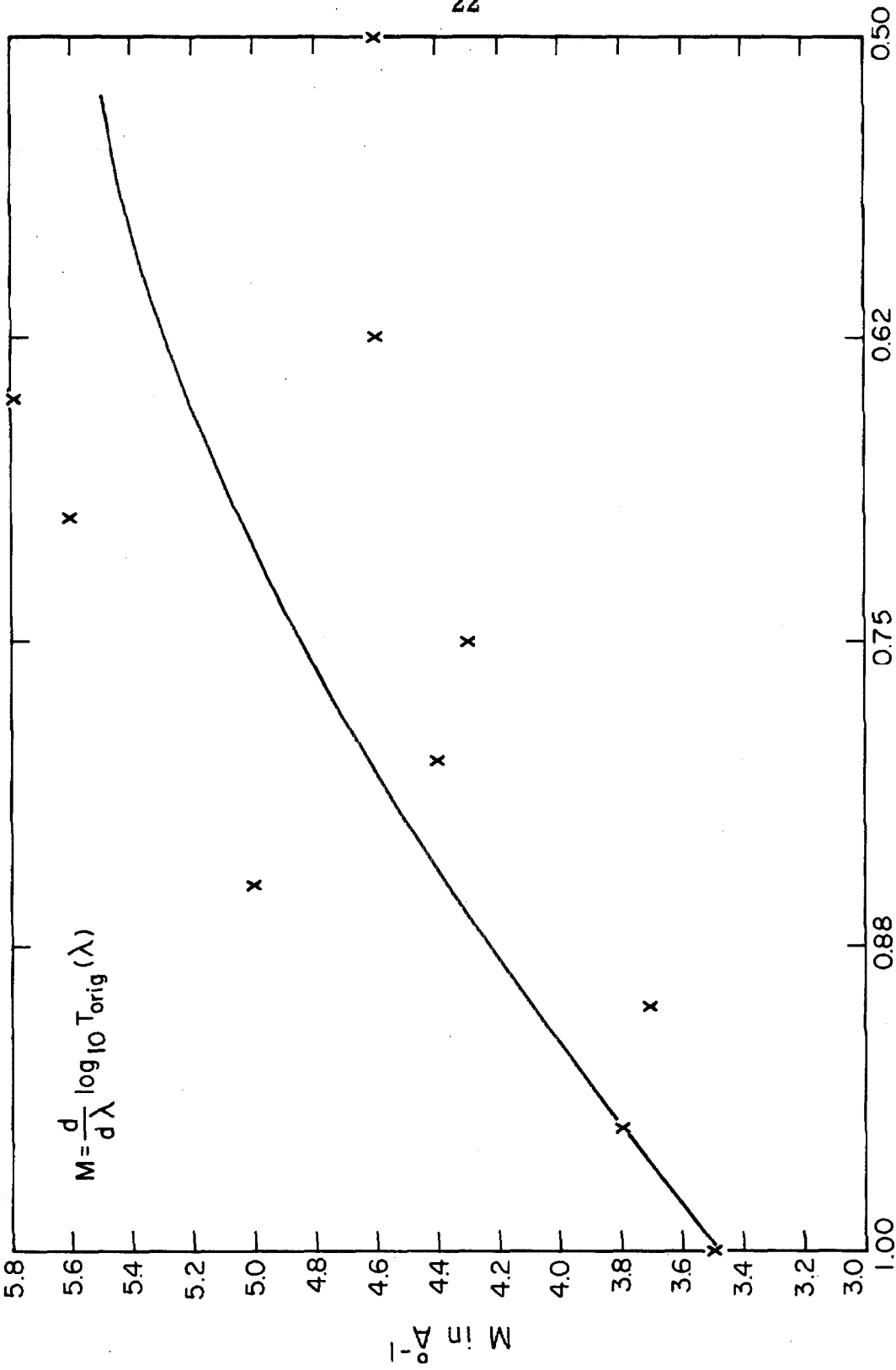distance from the disk center for the Z-photo of September 13,
1964.

21

Figure 2(a)

$$M = \frac{d}{d\lambda} \log_{10} T_{orig}(\lambda)$$

sin θ
Figure 2(b)

22

First consider the photographic contrast γ_M. Figure 3(a) and Figure 3(b) show characteristic curves for the original plates of August 16, 1964 and September 20, 1963 respectively. These curves were obtained from microphotometer tracings of calibrated stepwedges on the respective plates. Sunspots appear on both plates, and the typical exposures of the umbras and penumbras of these spots together with the exposures of the average solar disk are indicated on the characteristic curves. Note that the linear portions of the curves in Figure 3(a) and Figure 3(b) have equal slopes, the common value being $\gamma_M = 2.5$. In each figure, the exposure of the average solar disk falls on the linear portion of the curve where $\gamma_M = 2.5$. The sunspots that appear on the plate of August 16, 1964 are relatively small (area $\sim 0.4 \times 10^{18} cm^2$) and have very little or no penumbras. We see in Figure 3(a) that the exposure of the penumbras falls on the linear portion of the curve where $\gamma_M = 2.5$, whereas the exposure of the umbras lies slightly off the linear portion where $\gamma_M = 1.7$. The sunspots that appear on the plate of September 20, 1963 are relatively large (area $\sim 30 \times 10^{18} cm^2$) and have extensive penumbras. We see in Figure 3(b) that the exposure of the penumbras falls off the linear portion of the curve only very slightly, γ_M being 2.1. However, the exposure of the umbras of September 20, 1963 lie well off the linear portion of the curve where $\gamma_M < 0.1$. Thus, typically one might expect the photographic contrast γ_M for the average solar disk to be the same as for the penumbras of even the large sunspots within approximately 15% and for the umbras of small sunspots within about 30%. One would expect the photographic contrast of the umbras of large sunspots to be essentially zero. Z-photos show

Figure 3

(a)   Characteristic curve for the original Zeeman plate of
      August 16, 1964. $\frac{I_s}{I_0}$ is proportional to the exposure,
      and 0 is the opacity of the original plate. γ refers to the
      slope of the characteristic curve.

(b)   Characteristic curve for the original Zeeman plate of
      September 20, 1963. The notation is the same as in
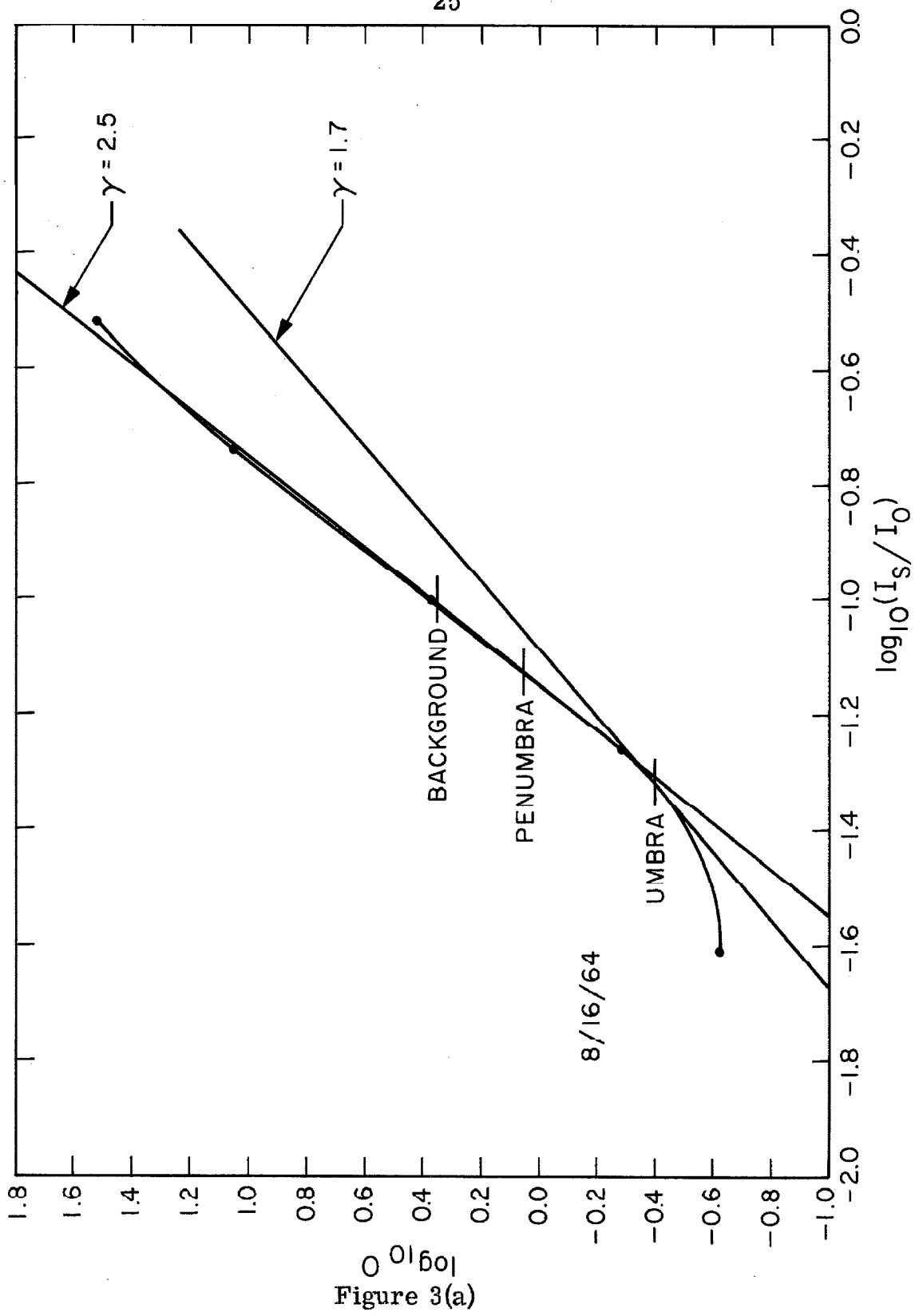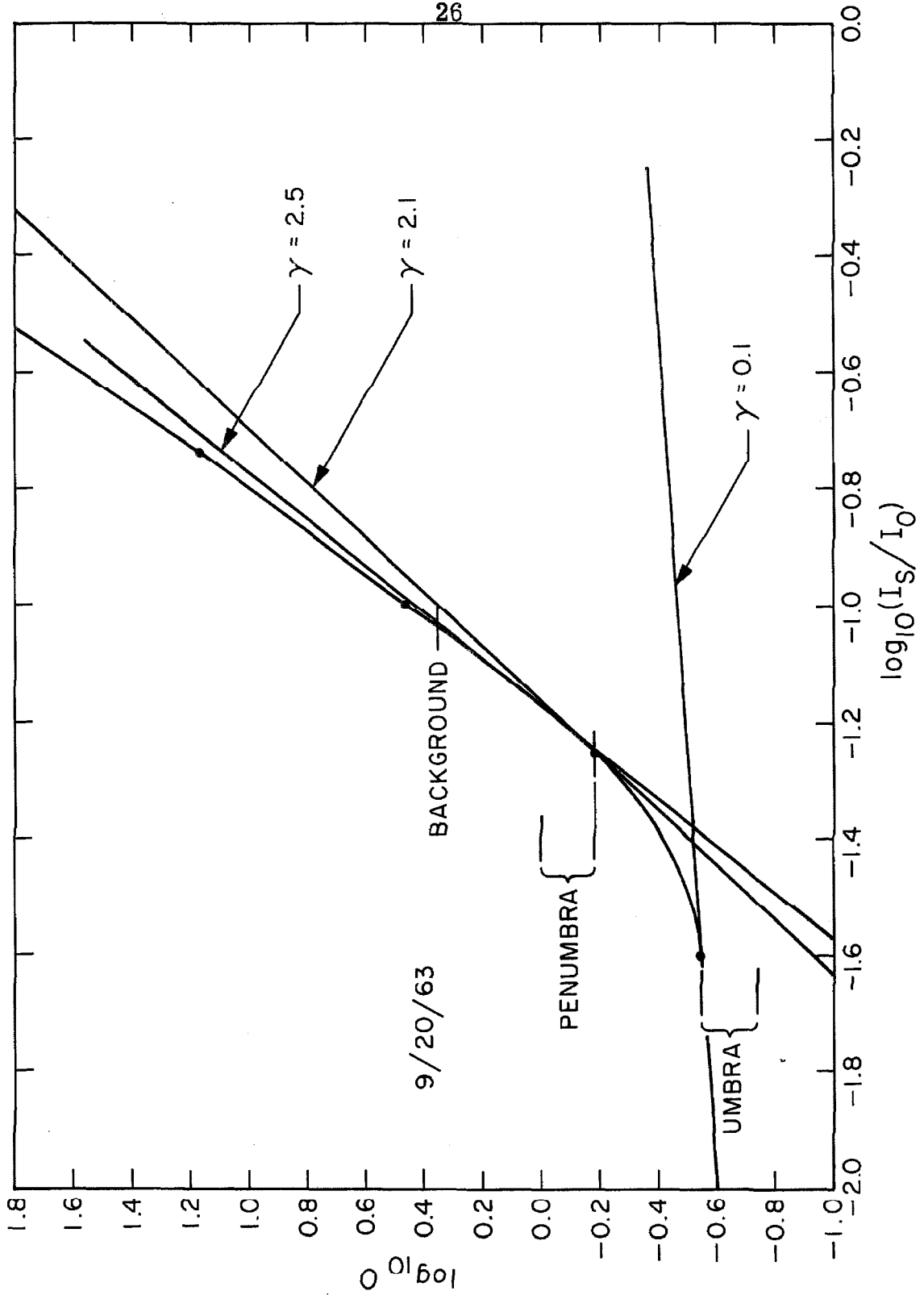   Figure 3(a).

Figure 3(a)

Figure 3(b)

fields in the penumbras of even the large sunspots and the umbras of small sunspots, but show no fields at all in the umbras of large sunspots, in qualitative agreement with our expectations. Finally, we note from Figure 3(a) and Figure 3(b) that in each case it would have been possible to increase the average exposure of the plate by a factor of 1. 5 - 2. 0 without shifting off the linear portion of the curve. This would have increased the sensitivity toward fields in sunspots without changing the sensitivity toward fields outside sunspots. Since we did not wish to widen the slits further, this meant increasing the exposure time. This, in turn, would have taken up more of the precious period of good seeing than it seemed worth. Hence we exposed the plates just enough to permit measurement of non-spot fields, and not much more.

Next consider the spectral sensitivity, $\frac{I_0'(\lambda)}{I_0(\lambda)}$. The lack of knowledge of sunspot spectra makes an evaluation of $\frac{I_0'(\lambda)}{I_0(\lambda)}$ very difficult. Visual inspection of the Mount Wilson Photographic Map of the Sunspot Spectrum suggests that the $\lambda 6103$ line is deepened and widened in sunspots, as do the Rowland Intensities of 9 on the disk and 25 in spots (14). This might lead one to suspect that $\frac{I_0'(\lambda)}{I_0(\lambda)}$ would be smaller for sunspots than for the average solar disk. Rather than speculate further, we shall now consider two rather crude measurements of the combined photographic and spectral sensitivity to magnetic fields in sunspots compared to the sensitivity to fields not in sunspots.

It was noticed that two of the small sunspots of August 16, 1964 had roughly the same transmission on spectroheliograms taken on

the wing of the λ6103 profile. These two sunspots had opposite magnetic polarities so the transmission of one sunspot on a spectroheliogram exposed to right-hand circularly polarized light was compared with the transmission of the other sunspot on a spectroheliogram exposed to left-hand circularly polarized light. The transmissions were compared visually. It was also noticed that both of these spots appeared on the expanded line profile, one appearing in the core of the line and the other appearing approximately 0.12A to the violet of the line core. The transmissions of these two spots on the expanded line profile together with the transmissions of the average solar disk were then measured photoelectrically with the results shown in Table 1.

TABLE 1

	spot	disk
core	9.5	3.9
wing	3.0	1.0

Using the transmissions in Table 1, one obtains

$$\frac{(\frac{\Delta\log_{10}T}{\Delta\lambda})_{spot}}{(\frac{\Delta\log_{10}T}{\Delta\lambda})_{disk}} = 0.85.$$ A similar procedure was carried out for

the penumbra of the large sunspots of September 20, 1963 with the transmissions shown in Table 2.

TABLE 2

	penumbra	disk
core	7.0	3.0
wing	2.5	0.9

Using these transmissions, one obtains

$$\frac{\left(\dfrac{\Delta\log_{10}T}{\Delta\lambda}\right)_{penumbra}}{\left(\dfrac{\Delta\log_{10}T}{\Delta\lambda}\right)_{disk}} = 0.86,$$ fortuitously close to the value of 0.85

just obtained for the umbra of the small spots of August 16, 1964. No attempt will be made to estimate the error of these measurements in view of the rather crude procedure of obtaining them. Rather, let us say that these results are not inconsistent with the following statement. The method of using the expanded line profile of the average solar disk to calibrate magnetic fluxes in the umbras of small sunspots and in the penumbras of even the large sunspots will result in values perhaps too small by less than 50%, whereas the method will not yield any magnetic flux at all in the umbras of large sunspots.

D. Sources of Error

The precision of the magnetic flux measurements described here is limited by several sources of error. In this section we shall consider the chief sources of error and then attempt to summarize the accuracy of the flux measurements.

The largest source of error was the variation of the zero-field transmission on each Zeeman plate. The basic procedure was to measure $C = \int_{A_0} TdA$ and $C_0 = \int_{A_0} T_0 dA$, the integrated transmissions for the field region of interest and for a nearby zero-field region, respectively. The magnetic flux was then obtained from the quantity $A_0 R = A_0 \left(\dfrac{C - C_0}{C_0} \right)$ as described in Part II (B). The variation of the zero-field transmission resulted in an uncertainty in the value of C_0 which in turn produced an uncertainty in the measured magnetic flux. If the variation in C_0, ΔC_0, was much less than $C - C_0$ for a given magnetic feature, then the percent error in the flux measurement was quite small. Except for magnetic features having fluxes comparable to the threshold values (typically $\Phi_{||} \sim 0.1$ SFU), the error was kept less than approximately $\pm 25\%$ by a suitable choice of photometer aperture A_0. However, for magnetic features having fluxes comparable to the threshold value, the error was roughly $\pm 100\%$ corresponding to $A_0 R \sim 0.3 \pm 0.3$ mm^2 for which typically $\Phi_{||} \sim 0.1 \pm 0.1$ SFU. As an illustration, consider the procedure of obtaining the flux in a typical BMR: Starting with large patches of strong fields, relatively large apertures are used resulting in flux signals large compared to the noise level variations of the zero-field regions. The percent error in the flux measurement is generally less than $\pm 20\%$. As one measures progressively smaller patches of flux using the large apertures, eventually the flux signal becomes comparable to the noise level variations in which case the percent errors in the flux measurements are intolerable. Smaller apertures are then used, increasing the signal-to-noise ratio with a corre-

sponding reduction in the percent errors in the flux measurements.
This procedure of using progressively smaller apertures to measure
the fluxes of progressively smaller magnetic features is continued
until the magnetic features are so small that their flux signals are
comparable to the noise level variations for the smallest aperture
used (2mm x 2mm). This is the threshold of flux measurement and
corresponds to $A_0 R \sim 0.3 \pm 0.3$ mm^2 for which typically
$\Phi_{\parallel} \sim 0.1 \pm 0.1$ SFU as mentioned above. The magnetic <u>fields</u> of
even these very small magnetic features can be measured by using
the much smaller aperture of a microphotometer. This has been
done for several such very small magnetic features and the results
are described in Part III (C).

A second source of error occurred in the measurement of the
calibration factor $\dfrac{d \log_{10} T_{orig}(\lambda)}{d\lambda}$ from the expanded line profiles.
Repeated measurements of $\dfrac{d \log_{10} T_{orig}(\lambda)}{d\lambda}$ for the same disk
position on a given plate yielded a scatter of roughly $\pm 10\%$. The
measurements of Figure 2(b) of Part II (C), in which $\dfrac{d \log_{10} T_{orig}(\lambda)}{d\lambda}$
is plotted versus disk position, also show a scatter of approximately
$\pm 10\%$. There was considerable variation of $\dfrac{d \log_{10} T_{orig}(\lambda)}{d\lambda}$ from
plate to plate, the values ranging from $3A^{-1}$ to $8A^{-1}$. This was
because $\dfrac{d \log_{10} T_{orig}(\lambda)}{d\lambda}$ includes the effects of several factors such
as slit widths; position of the exit slit on the line profile; variation
of the line profile from disk center to limb; curvature and tilt
of the line; sensitivity, exposure, and development of the original
photographic plate; atmospheric transparency and scattered light.

The calibration curves obtained from the expanded line profiles
were linear over a considerable range of wavelength, and for the
plates reduced, the position of the exit slit with respect to the line
profile was such that changes in $\log_{10}T_{orig}(\lambda)$ were linear for
fields up to $\pm$ 1000 gauss, and many of these were linear for fields
as large as 1500-2000 gauss.

A third source of error was the reduction of the Z-photos
from the original plates. Simon (10) considered the error introduced
by deviations from unity gamma in the various stages of photographic
reduction, and estimated a 20-30% error for his reductions. With
this in mind, special care was used in the reduction of the Z-photos
described here. All of the contact prints obtained in the various
stages of reduction were individually checked for unity gamma by
placing plates in contact and looking visually for transmission
variations on the superimposed pairs. When no appreciable variation
could be seen the plates were retained for the next stage of
processing. However, if an appreciable variation was observed the
contact print was discarded and another made. Unfortunately the
projection printing could not be tested for unity gamma in this way.
The same exposure and development was used for the projection
printing as the contact printing and a contact print was generally
made and tested before the projection printing was started. A few
tests of the gamma of the projection printing were made in the
following way: A pair of Z-photos having reciprocal transmission
was used. One of these photos was projection printed with unit
enlargement and developed in the manner expected to produce unity
gamma. Then a contact print of this projection print was made in
the same way and checked for unity gamma. Finally the contact

print was placed in register with the other of the two original
Z-photos and the superimposed pair inspected visually. No
appreciable variation in transmission was observed for the few
such tests made, indicating that unity gamma had been achieved
in the projection printing. Let us now estimate the photographic
error: Proceeding in a manner similar to that of Simon (10), one
obtains for a Z-photo:

$$(15) \quad T/T_0 = \left[\frac{(1 - \delta)^{\gamma_1 \gamma_3 + \gamma_2 \gamma_4}}{(1 + \delta)^{\gamma_1 \gamma_2 \gamma_4 + \gamma_3}} \right]^{\gamma_5 \gamma_M}$$

where: T/T_0 is the transmission of the region of interest relative
to the zero-field transmission,

δ is proportional to the line-of-sight component of magnetic
field and satisfies

$$\delta = \Delta\lambda \cos\gamma \ \frac{I_0'(\lambda)}{I_0(\lambda)} \ \text{as defined in Part II (B)},$$

γ_M is the gamma of the original plate,

γ_1 is the gamma of the contact print of the original plate,

γ_2 and γ_3 are the gammas of the projection prints of the
singly cancelled plates,

γ_4 is the gamma of the contact print of one of the two
projection prints of the singly cancelled plates,

γ_5 is the gamma of the projection print of the doubly
cancelled plate.

Since all of these gammas except γ_M are approximately unity, let us express T/T_0 in terms of the deviations of these gammas from unity. In particular, defining ϵ_i, $i = 1, 2, \ldots 5$ by

$$(16) \quad \gamma_i = 1 + \epsilon_i, \quad i = 1, 2, \ldots, 5$$

and, neglecting terms in ϵ_i of order greater than first-order, one obtains:

$$(17) \quad T/T_0 = \left(\frac{1 - \delta}{1 + \delta}\right)^{2\gamma_M'},$$

where

$$\gamma_M' = \gamma_M(1 + \epsilon)$$

and

$$\epsilon = \frac{1}{2}\left(\epsilon_1 + \epsilon_2 + \epsilon_3 + \epsilon_4\right) + \epsilon_5.$$

Now assuming all of the errors ϵ_i are as large as 5% and that, at worst, they all have the same sign, one obtains

$\epsilon = \frac{1}{2}(5 + 5 + 5 + 5) + 5 = 15\%$ as an upper limit of the typical error introduced in the photographic reduction. At worst, the gammas of the projection prints might be as much as 1.2, and in such a case one would have $\epsilon \sim \frac{1}{2}(5 + 20 + 20 + 5) + 20 = 45\%$ making the measured fields too large by at most 45%.

A fourth source of error was introduced by the approximation $(A_0 R)_{GM} = \int_{A_0} (4\gamma_M \delta)dA$ (see Part II (B)). This error is described in detail in Appendix II. It causes the measured fluxes to be too large, and although the error depends on the amount of flux measured, it is typically less than 6%.

A fifth source of error was the accuracy to which the photo-
meter apertures were known. The apertures were obtained in the
rather crude manner of cutting square holes in black cardboard
using an X-acto knife. Although the percent error in the aperture
area presumably varied with the area, being smallest for the largest
aperture and largest for the smallest aperture, typically one might
expect an error less than $\pm$ 5%.

A sixth source of error occurred in plate registration at the
various stages of reduction of the Z-photos. First, a very slight
difference in the lateral magnification (roughly 1.000 compared to
1.004) in the two light paths produced images that differed slightly
in their lateral dimension on the original plate. This has been
described by Leighton (1) and Simon (10). As a result, satisfactory
registration could be obtained over only a limited portion of the
image at the singly cancelled stages of reduction. This was not a
serious problem since the region of interest was generally smaller
than the size of a region that could be satisfactorily cancelled, and
the single cancellations were made to give the region of interest the
best possible registration. Second, because doubly-cancelled plates
were obtained by combining singly-cancelled plates taken at different
times, accurate guiding of the solar image and good atmospheric
seeing conditions were important. To minimize fluctuations due to
atmospheric seeing, the plates were exposed generally within an hour
after sunrise. However, at this time the gradually increasing light
intensity introduced a very small uniform drift in the guiding of the
east-west position of the solar image. This uniform drift was easily
compensated when necessary by shifting and tilting the singly-
cancelled plates slightly relative to each other before gluing to form
the doubly-cancelled plate. The maximum displacement of the singly-

cancelled images depended upon the exposure time and was generally less than 0.4 mm. This was enough to prevent cancellation of the streaks on the plate introduced by the polaroids, however. Nevertheless, these streaks were easily identifiable and did not affect the flux measurements. To avoid errors due to adverse seeing and poor guiding, plates containing considerable random seeing and guiding fluctuations comparable to the smallest resolvable features of interest were not measured. In general, these errors associated with plate registration tended to decrease the measured fields. Slight registration errors in the double cancellation process would not be expected to affect the flux measurements provided the fields do not thereby drop below threshold. This can be seen from the following simple example. Consider a doubly-cancelled plate formed by the superposition of two singly-cancelled plates. Suppose that the singly-cancelled plates are not quite in register so that a magnetic feature of area A on each singly-cancelled plate does not overlap perfectly in the doubly-cancelled plate (see Figure 4).
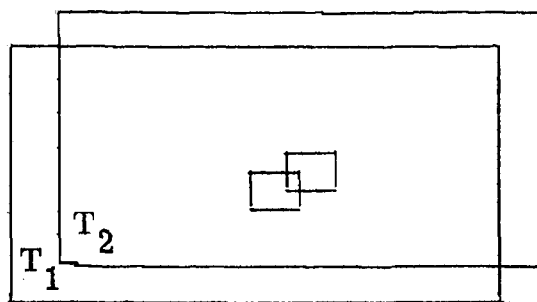

Figure 4

Call the area of overlap B. If the transmissions of the two plates

are $T_1 = T_{10} \left(\frac{1 + \delta}{1 - \delta} \right)^{\gamma_M}$ and $T_2 = T_{20} \left(\frac{1 + \delta}{1 - \delta} \right)^{\gamma_M}$, respectively, then the zero-field transmission on the doubly-cancelled plate will be $T_0 = T_{10}T_{20}$, the transmission of the overlap region will be

$T_B = T_{10}T_{20} \left(\frac{1 + \delta}{1 - \delta} \right)^{2\gamma_M}$, and the transmission of the non-overlapping field regions will be $T_A = T_{10}T_{20} \left(\frac{1 + \delta}{1 - \delta} \right)^{\gamma_M}$. For small fields, this leads to $\frac{\Delta T_A}{T_0} = 2\gamma_M\delta$ and $\frac{\Delta T_B}{T_0} = 4\gamma_M\delta$ so that the measured field in the non-overlapping region is half the measured field in the overlapping region. However, the flux of the entire field region will be proportional to

$$(A - B)(2\gamma_M\delta) + B(4\gamma_M\delta) + (A - B)(2\gamma_M\delta) = (4\gamma_M\delta)(A) ,$$

independent of the overlap area B. This implies that the measured flux does not depend on the amount of overlap so that slight seeing and guiding fluctuations, giving rise to small errors in registration, would not be expected to affect the flux measurements. In practice, however, the variable zero-field transmission tends to wash out misaligned weak fields so that the flux measurements are likely to be somewhat reduced.

Next let us attempt to summarize the accuracy of the measurements of magnetic flux. We have considered the six chief sources of error:

1. variations in the noise level on Z-photos ($< 25\%$ for $\Phi_{\parallel} \gtrsim 0.5$ SFU and $\pm 0.1 - 0.2$ SFU for $\Phi_{\parallel} \lesssim 0.5$ SFU)

2. measurement of $\dfrac{d\log_{10}T_{orig}(\lambda)}{d\lambda}$ ($< 10\%$)

3. probable photographic reduction errors ($\lesssim 15\%$)

4. the approximation $(A_0 R)_{GM} = \displaystyle\int_{A_0} (4\gamma_M{}^\delta)dA$ ($\lesssim 5\%$)

5. accuracy of the photometer aperture areas A_0 (5%)

6. registration problems caused by

    (a) difference in image size (0%)

    (b) atmospheric seeing conditions

    (c) guiding fluctuations

Neglecting sources 4, 5 and 6, one obtains a total absolute error of approximately $\pm$ 50%. The scatter obtained in the flux measurements from day-to-day and plate-to-plate was closer to $\pm$ 30% than $\pm$ 50% so that we shall estimate a combined absolute error of 30 - 50%, realizing in addition that resolution and registration problems may cause the measured fields and fluxes to be too small in practice. Fluxes of different magnetic features or regions on a given Z-photo may be compared much more precisely than with 30 - 50% accuracy because the noise level variations are the only appreciable source of relative error. Thus, for example, differences in the measured fluxes in the leading and following parts of a BMR of as much as a factor of two are probably real.

III. The Measurements

A. Fluxes in BMRs

Regarding sunspot groups as sources of magnetic flux, we shall now attempt to discover how much flux is associated with various sunspot groups. Anticipating that the large sunspot groups have more magnetic flux than the small ones, we shall adopt sunspot area as a parameter to describe sunspot groups and in terms of which to present flux measurements. More precisely, we shall consider magnetic fluxes of BMRs as a function of A_m, the area of the solar surface covered by all the sunspots (umbras and penumbras of both leading and following parts) of the associated sunspot group at the time when this area is largest.

Magnetic fluxes were measured for eight BMRs either while there were sunspots or just after the sunspots had disappeared. In addition, the magnetic flux was measured for a short-lived BMR for which no sunspot was ever seen on plates taken daily at Mount Wilson. Whenever possible, the magnetic flux measurements were supplemented by sunspot umbral fluxes calculated from Mount Wilson magnetic observations of sunspots using the formula:

$$(18) \qquad \Phi_u = \sum_{i=1}^{N} B_i A_i \, ,$$

where

Φ_u is the flux due to the umbras of all the sunspots of a given magnetic polarity,

B_i is the measured field strength at the center of the umbra of the ith sunspot having the given magnetic polarity,

A_i is the area of the umbra of the ith sunspot,

N   is the number of sunspots having the given magnetic polarity.

The fluxes in penumbras were not included on the hypothesis that the photographic technique satisfactorily measured penumbral fluxes, and that supplementing our measurements with penumbral fluxes calculated from the Mount Wilson measurements would be redundant. The umbral areas A_i were obtained from Mount Wilson integrated light photographs by direct measurement with a ruler, and probably are not accurate within more than $\pm$ 20%. The values of A_m were also obtained this way, and therefore have the same $\pm$ 20% accuracy.

Most of the magnetic flux measurements were obtained from BMRs near the disk center so that no foreshortening corrections were necessary. However, on four days, measurements were made for BMRs greater than 50 degrees from the disk center. To correct for foreshortening, the areas of sunspots in these BMRs were multiplied by $(\frac{1}{\cos \theta})$ where θ was the heliocentric position of each of the BMRs on the solar disk. Likewise, the measured sunspot field strengths were multiplied by $(\frac{1}{\cos \theta})$ to obtain the fields normal to the solar surface. Together these corrections correspond to multiplying the sunspot flux by $(\frac{1}{\cos \theta})^2$. On this basis, the measured magnetic fluxes in the BMRs were multiplied by $(\frac{1}{\cos \theta})^2$ to correct for magnetic foreshortening.

The magnetic flux measurements for the eight BMRs together with three magnetic flux measurements of Bumba (15) are presented in Table 3. The first column identifies each BMR in terms of the Mount Wilson number of the associated sunspot group. The second

TABLE 3

group number	date of observation				Φ_m^l	Φ_m^f	Φ_u^l	Φ_u^f	A_s^l	A_s^f	A_m	Φ
	Φ_m	Φ_u	A_m	A_s			-1.5_{fc}	$+2.4_{fc}$	8.2	5.6		
12473	7/13/57	7/12/57	7/14/57	7/12/57	-15_{vb}	$+14_{vb}$	-1.9	$+2.1$	6.9	8.7	15.6	14.5_{vb}
12514	8/1/57	8/1/57	7/4/57	8/1/57	-33_{vb}	$+34_{vb}$	-8.4	$+0.2$	23.4	2.1	30.9	33.5_{vb}
12580	8/29/57	8/29/57 8/30/57	8/29/57	8/29/57 8/30/57	$>(50)_{vb}$	$>(50)_{vb}$	$+4.2$ $+4.4$	-4.0 -5.3	18.2 16.4	23.9 16.6	42.1	50_{vb}
15767	9/16/63	9/16/63	9/15/63	9/15/63 9/16/63	-8.5_a	$+12.7_a$	-1.6	$+0.0$	6.8 6.0	3.4 1.0	10.2	11.4_a
15768	9/20/63	9/20/63	9/20/63	9/20/63	$+21.4$	-10.8	$+1.1_b$	-8.2_b	19.3	20.0	39.3	20.8
15836	6/15/64	6/15/64	6/13/64	6/15/64	$+2.1$	-1.8	$+0.0$	-0.0	0.0	0.0	1.3	1.9
15845	7/16/64	7/16/64	7/14/64	7/16/64	-1.1_c	$+2.1_c$	-0.1_c	$+0.0_c$	0.2	0.0	1.1	1.6
15851	8/13/64	8/13/64	8/15/64	8/13/64	-6.4_{fc}	$+7.6_{fc}$	-3.7_{fc}	$+2.1_{fc}$	2.8_{fc}	2.4_{fc}	8.8_{fc}	9.9_{fc}
15852	8/14/64 8/15/64 8/16/64 8/17/64 8/19/64	8/17/64	8/15/64	8/17/64	$+2.8$ $+2.2$ $+4.3$ $+2.7$ $+3.8_{fc}$	-2.3 -1.9 -5.1 -3.6 -3.2_{fc}	0.1	no spot	0.2	no spot	1.8	4.7
BMR	8/15/64	-	-	-	-0.2	$+0.1$	-	-	-	-	0.0	0.2
15854	9/7/64 9/8/64 9/9/64	9/7/64	9/10/64	9/7/64	-0.5 -0.8 -1.8	$+0.9$ $+1.2$ $+2.0$	0.2	0.0	0.3	0.0	1.0	1.9
15855	9/12/64 9/13/64	9/13/64	9/13/64	9/13/64	$+0.6$ $+2.3_{fc}$	-0.7 -1.0_{fc}	$+0.4_{fc}$	-0.6_{fc}	0.4_{fc}	0.7_{fc}	1.1_{fc}	2.2_{fc}

42

Footnotes for TABLE 3

fc   indicates that a foreshortening correction has been made.

BMR   denotes a BMR in which sunspots were never seen at Mount Wilson.

vb   indicates flux measurements obtained by V. Bumba (15).

a   The flux of MWO group 15767 could not be isolated with certainty from the flux of a nearby BMR.

b   Since there were no Mount Wilson magnetic field strength measurements for 9/20/63, the field strengths were estimated from the sunspot areas and the known magnetic field strength versus sunspot area relation (equation (20) of the text and references (16) and (17)).

c   On 7/16/64 a small BMR with no sunspots was located 160,000 km due west of MWO group 15845. The BMR was also out of flux balance with leading and following fluxes of -1.6 SFU and $+0.3$ SFU, respectively. If MWO group 15845 and the small BMR are taken together, the flux of the combination balances within measurement accuracy, the leading and following fluxes being -2.7 SFU and $+2.4$ SFU, respectively.

column contains the dates on which the magnetic flux measurements
were made. The third column contains the dates for which the
umbral sunspot fluxes were calculated from the Mount Wilson
magnetic observations. The fourth column contains the dates on
which A_m was measured. The fifth column contains the dates on
which the total (umbra plus penumbra) sunspot areas for leading
and following sunspots, respectively, in each group were measured.
The sixth and seventh columns contain the measured magnetic fluxes
for the leading and following parts of each BMR respectively. A
positive sign corresponds to a magnetic vector directed toward the
observer and a negative sign corresponds to a magnetic vector
directed away from the observer. The eighth and ninth columns
contain the umbral fluxes calculated from the Mount Wilson magnetic
observations of sunspots for the leading and following sunspots,
respectively, of each group. The signs have the same meaning as
in the sixth and seventh columns. The tenth and eleventh columns
contain the total sunspot areas (umbra plus penumbra) of all the
leading and following sunspots, respectively, of each group. The
twelveth column contains the parameter A_m defined above. The
thirteenth column contains the source fluxes of the BMRs. The
source flux of a BMR was taken to be the average of the absolute
values of the total fluxes (measured flux plus calculated sunspot flux)
of leading and following magnetic polarities on the day for which this
average was largest. The source fluxes for Bumba's measurements
do not include the calculated sunspot fluxes since he claimed (15)
that his measurements included sunspot flux. (Since the calculated
umbral fluxes are small compared to Bumba's measurements, it
makes no appreciable difference whether the umbral fluxes are
included in the source fluxes or not.) In Table 3, all fluxes are

expressed in SFU and all areas are expressed in units of 10^{18}cm^2.

Figure 5 shows the source fluxes, Φ, plotted versus A_m for the BMRs of Table 3. Only two of the twelve points deviate appreciably from the straight line, $\Phi = 1.2 A_m$, over the entire range of source fluxes from 0.0 SFU to 50.0 SFU. Neither of these two points represent measurements of Bumba (15), his measurements of very large source fluxes and our measurements of medium and small source fluxes falling along the same straight line. The two points that do deviate appreciably from the straight line correspond to groups 15768 and 15852, the measured source fluxes of groups 15768 and 15852 being appreciably lower and higher, respectively, than the corresponding fluxes on the straight line.

The flux associated with group 15768 was measured on September 20, 1963 when its sunspot area was maximum. If the photographic technique did not measure an appreciable fraction of penumbral flux as well as no umbral flux, one might expect our measured magnetic flux to be too low. Let us estimate how much larger the source flux might be on this basis:

Mattig (18) measured the distribution of magnetic field over sunspots and then integrated this distribution (17, 18) to obtain:

$$(19) \quad \Phi = 0.25 \, B_0 A$$

as the formula for the magnetic flux, Φ, in a sunspot as a function of the field B_0 at the center of its umbra and the area, A, of its umbra plus penumbra. We shall use this formula to estimate the total sunspot flux of each polarity for group 15768, realizing that our result will not be very accurate since group 15768 was a complicated γ-group whereas Mattig's results were obtained for

Figure 5

Source fluxes, Φ, plotted versus sunspot group size A_m
for the BMRs of Table 3. NRS refers to our measurements
and VB refers to the measurements of Bumba (15).
(1 SFU = 10^{21} maxwells.) There are four points in the un-
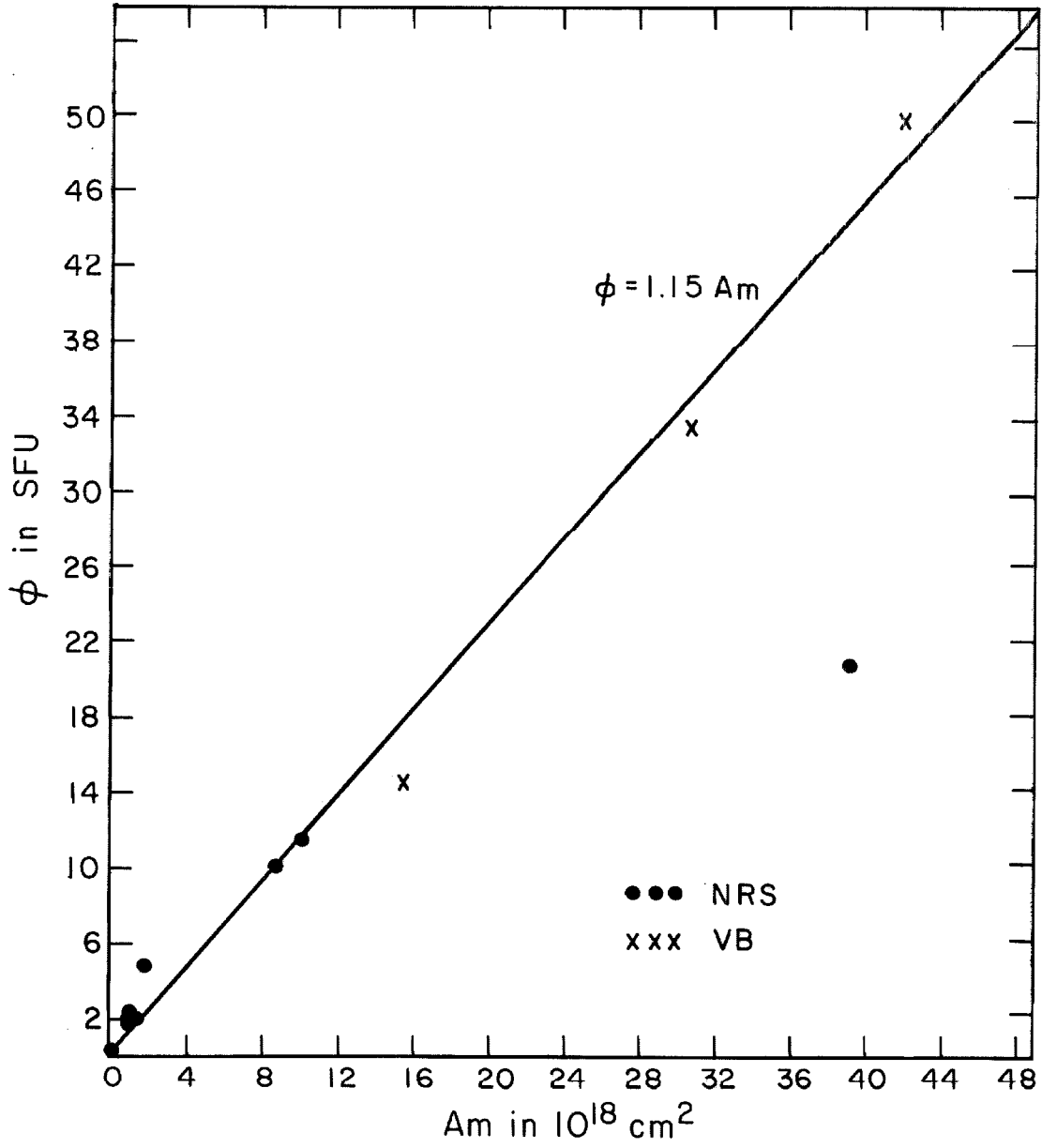resolved cluster at $\Phi \sim 2$ SFU.

Figure 5

isolated, large, stable sunspots. From Table 3, $A \sim 20 \times 10^{18} \text{cm}^2$.
Since B_0 was not measured at Mount Wilson on September 20, 1963,
let us estimate B_0 knowing the sunspot area, A. Houtgast and
Van Sluiters (16, 17) found that for sunspots near the disk center:

$$(20) \quad B_0 = 3700 \left(\frac{A}{A + 66} \right) \text{ gauss,}$$

where A is the sunspot area (umbra plus penumbra) in units of
$10^{-6} \times 4\pi R^2$, R being the solar radius. Converting $A = 20 \times 10^{18} \text{cm}^2$
into units of $10^{-6} \times 4\pi R^2$, one obtains $B_0 \approx 3000$ gauss from
equation (20). Using equation (19), we then obtain
$\Phi = 0.25 \times 3000$ gauss $\times 20 \times 10^{18} \text{cm}^2 \sim 15$ SFU as the sunspot
flux of each magnetic polarity in group 15768. Since the photo-
graphically-obtained fluxes for this group were supplemented by
only +1.1 SFU and -8.2 SFU in the leading and following parts
respectively, it is possible that the source flux could be increased
by 10-15 SFU bringing it to 30-35 SFU.

Although the source flux of group 15852 was obtained from the
measurements of August 16, 1964, flux measurements of this group
were also obtained on August 14, August 15, August 17 and
August 19. Table 3 shows that the flux measurements of August 16
were roughly 1.0 SFU larger than the typical fluxes for the other
four days despite the fact that the sunspot area reached maximum
on August 15 and had decreased considerably by August 19. The
relatively large source flux of this group may therefore be due to
a random error, a more accurate estimate being about 1.0 SFU
lower, and hence roughly within the expected deviation from the
corresponding source flux on the straight line, $\Phi = 1.2 \, A_m$.

Summarizing Figure 5, the source flux of a sunspot group is roughly equal to the maximum area it ever attains if the magnetic flux and area are expressed in SFU and $10^{18} cm^2$, respectively.

The photographically-obtained fluxes of leading and following polarity were compared for each BMR measured. The only detectable imbalances occurred during the forming and decaying stages of the BMRs, no appreciable imbalance being found during most of the observable lifetime of each BMR.* It was difficult to study the flux imbalance during the decaying stage since much of the flux is then below the measurement threshold. However, the fluxes during the forming stage of the BMRs were studied, and imbalances were found to occur only while sunspots were present in the BMRs. Whenever an imbalance of photographically-obtained flux occurred, the sunspot fluxes calculated from the Mount Wilson magnetic observations were also out of balance such that the magnetic polarity of smaller photographically-obtained flux had the larger calculated sunspot flux.

Table 4 contains a summary of the relative fluxes of leading and following magnetic polarity for some of the BMRs listed in Table 3. The first column identifies each BMR in terms of the Mount Wilson number of the associated sunspot group. The second column contains the dates on which the flux measurements were made. The third column contains the heliographic location of the BMR on the day that the measurements were made. The fourth

---

*An exception to this was observed on July 16, 1964 in which two neighboring BMRs were each out of flux balance. However, the flux of these two BMRs taken as a unit was in balance.

TABLE 4

group number	date of observation	position of group	$\Delta\Phi_u$	$\Delta\Phi_m$
15767	9/16/63	S10, W10	+1.6	- 4.2$_a$
15768	9/20/63	N13, W3	-7.1	+10.6
15836	6/15/64	N6, E18	0.0	+ 0.2
15845	7/16/64	N28, E13	+0.1$_b$	- 1.0$_b$
15851	8/13/64	N22, W42 fc	+1.6$_{fc}$	- 1.2$_{fc}$
BMR	8/15/64	N9, E36	+0.1	0.0
15852	8/17/64	N8, W19	+0.1$_c$	- 0.9$_c$
15854	9/7/64	N39, W17	+0.2	- 0.4
15855	9/13/64	N7, W50 fc	-0.2$_d$	+ 1.3$_d$

Footnotes to Table 4

fc   indicates that a foreshortening correction has been made.

a   The flux of MWO group 15767 could not be isolated with certainty from the flux of a nearby BMR.

b   It is possible to explain this imbalance in terms of a similar imbalance in a nearby BMR (see footnote c of Table 3).

c   The flux of leading magnetic polarity was spread out considerably more than the flux of following polarity. Therefore, one might expect relatively more flux of leading polarity to be undetectable below the measurement threshold than flux of following polarity. This might in part explain the difference in magnitudes of $\Delta\Phi_u$ and $\Delta\Phi_m$ for MWO group 15852.

d   The fluxes uncorrected for foreshortening were

$$\Phi^l = \Phi^l_m + \Phi^l_s = 0.9 + 0.1 = 1.0 \quad \text{and}$$

$$\Phi^f = \Phi^f_m + \Phi^f_s = 0.4 + 0.2 = 0.6 \text{ SFU.}$$ If the lines of force from the leading and following parts of the BMR were inclined toward each other approximately 14 degrees from the normal, this would account for the observed flux imbalance. The common value of flux normal to the surface would then be approximately 2.0 SFU.

$$\Delta\Phi_u = \left| \Phi^l_u \right| - \left| \Phi^f_u \right|$$

$$\Delta\Phi_m = \left| \Phi^l_m \right| - \left| \Phi^f_m \right|.$$

column contains $\Delta\Phi_u = |\Phi_u^l| - |\Phi_u^f|$, the excess of calculated umbral flux of leading polarity over calculated umbral flux of following polarity. The fifth column contains $\Delta\Phi_m = |\Phi_m^l| - |\Phi_m^f|$, the excess of measured magnetic flux of leading polarity over measured flux of following polarity. We see in Table 4 that imbalances in photographically-obtained flux are generally accounted for by similar imbalances in calculated sunspot flux.

There are several factors which might affect the measurements in Table 4. First, the measurement of sunspot fields is not very accurate for small spots (area $\sim 0.4 \times 10^{18} cm^2$), the typical field strengths being 100-300 gauss with typical errors of 100-200 gauss depending on the observer's experience and bias (19). These errors are increased by adverse atmospheric seeing conditions. Second, the sunspot areas could be estimated only very roughly for the small sunspots. Third, the sunspot observations were generally made a few hours after the Z-photos were taken so that changes in sunspot activity during the few hours time would not be accounted for and would thus affect the comparison of fluxes.

In summary, within measurement accuracy, we find no imbalance of flux of leading and following magnetic polarity in the BMRs observed provided that the photographically-obtained fluxes are supplemented by the fluxes in the umbras of sunspots.

B. The Development of BMRs During the First Few Months
   Following Their Birth

The study of the development of BMRs is difficult for three
reasons. First, it is difficult to isolate one BMR from other mag-
netic regions. Second, solar rotation carries the BMR of interest
out of sight for a period of approximately fourteen days, during
which changes may occur in the BMR. Third, there is a tendency
for sunspots to recur in the vicinity of prior activity (6, 20, 21),
thus disturbing the development of the BMR of interest.

The summer and autumn of 1964 were opportune times for
studying the development of BMRs because the amount of solar
activity was relatively small. Thus, those BMRs that did occur
were relatively isolated. During the period June-October 1964,
observations were made nearly every day. A spectroheliogram
in the core of Hα was usually taken, and a Z-photo was obtained
on those days when magnetic regions of interest were on the solar
disk. Although information concerning the behavior of BMRs on
the time scales of days and minutes was obtained, we shall not
discuss it here. The diurnal changes of the magnetic field
patterns in BMRs have been described by Leighton (1).

The BMRs corresponding to Mount Wilson sunspot numbers
15851 and 15852 were followed for one and two solar rotations,
respectively. These two BMRs were traced from their initial
stages of compact appearance and sunspot activity to their later
stages of extended area without sunspots. A partial history of
these BMRs is summarized in Figures 6 and 7, respectively, in
which Z-photos and corresponding Hα spectroheliograms are
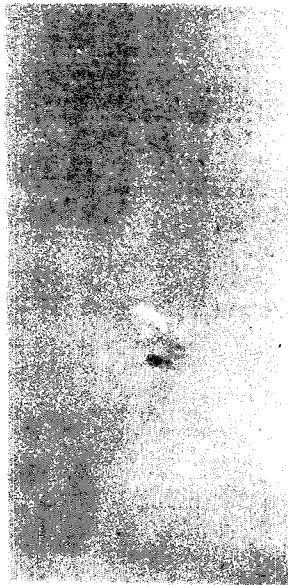shown for successive rotations. The magnetic fluxes have been

Figure 6

Photographs of the BMR associated with Mount Wilson sunspot group 15851. The upper photos were taken within a few days of the formation of the BMR, and the lower photos were taken during the next disk appearance. In the Z-photos, lighter-than-average features indicate positive magnetic polarity (magnetic vector directed toward the observer) and darker-than-average features indicate negative polarity (magnetic vector directed away from the observer). Φ_s refers to the source flux, and Φ_l and Φ_f refer to the absolute values of the total leading and following fluxes respectively. In each of the photographs north is roughly toward the top of the page, and east is to the right. On August 13, 1964, the BMR was located at roughly (22^ON, 42^OW). On September 9, 1964, the contiguous features of strong but opposite magnetic field were located at approximately (21^ON, 6^OE).

54

Figure 6

Figure 7

Photographs of the BMR associated with Mount Wilson sunspot group 15852. The upper photos were taken within a few days of the formation of the BMR, and the middle and bottom photos were taken during the second and third disk appearances respectively. In the Z-photos, lighter-than-average features indicate positive magnetic polarity (magnetic vector directed toward the observer) and darker-than-average features indicate negative polarity (magnetic vector directed away from the observer). Φ_s refers to the source flux, and Φ_l and Φ_f refer to the absolute values of the total leading and following fluxes of the BMR respectively. In each of the photos, north is roughly toward the top of the page and east is to the right. On August 16 the center of this BMR was located roughly at $(8^{\circ}N, 0^{\circ}EW)$. Note the small BMR about 3.5 cm on the page east of group 15852. This was a new-cycle BMR born on August 15. No sunspots were seen in this BMR at Mount Wilson. (see text, and Table 3). The small BMR does not appear striking on the Z-photo because of a slight plate misalignment during the reduction stages. On September 12, 1964, the center (indicated by the small disk filament on the Hα- SHG) of the BMR was roughly $(8^{\circ}N, 5^{\circ}W)$. (The center is located about 3 cm from the left edge of the photo.) On October 9, 1964, only a few scattered fragments of positive magnetic polarity remain. These are located on the page roughly 1 cm from the right border of the photos, and about 3 cm down from the upper border. On the sun they are located at roughly $(8^{\circ}N, 11^{\circ}W)$. Although one would expect the following portion of this BMR in the lower photos to be out of sight off the right edge, very little evidence for the following portion was indicated on either the full disk in Hα or other Z-photos, suggesting that this portion had either merged with the background field or fallen below the threshold of detectability.
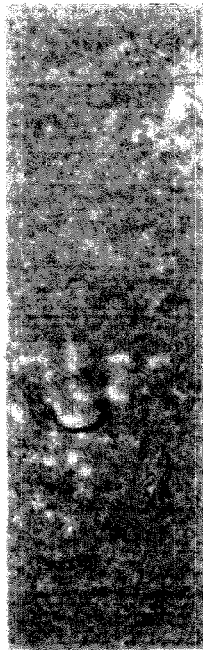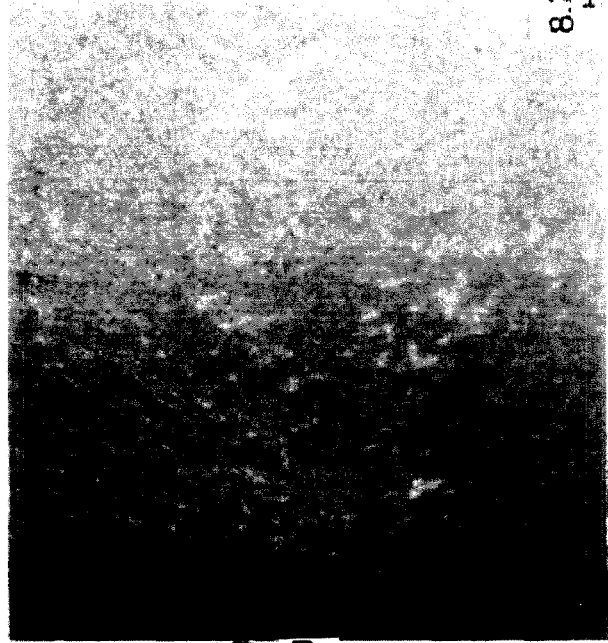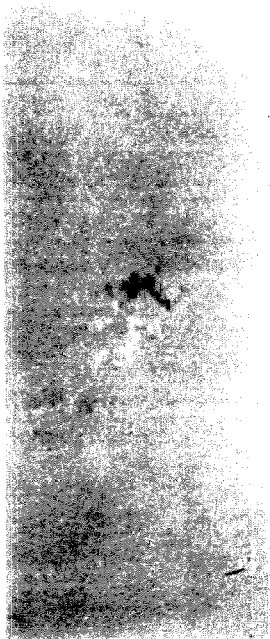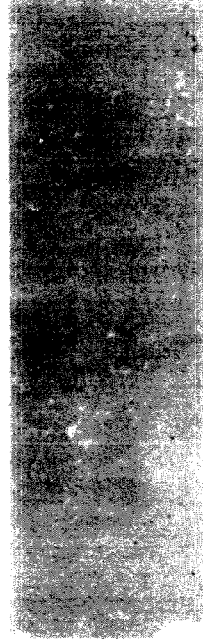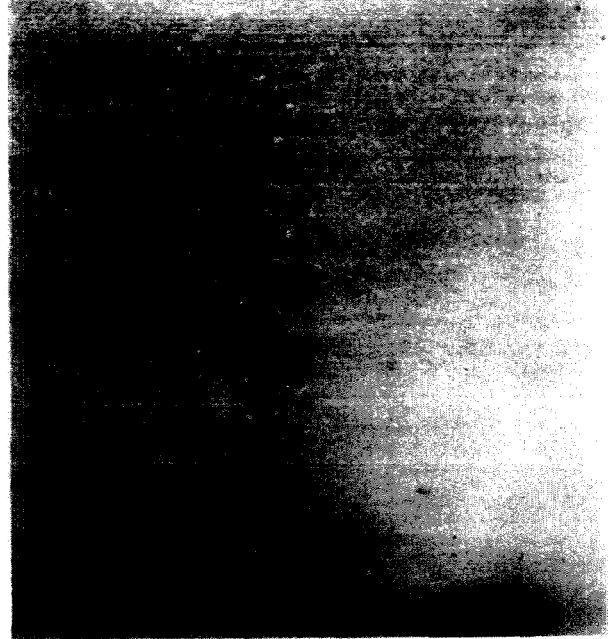
Figure 7

measured for these BMRs, and are recorded next to the corresponding Z-photos.

In an attempt to compare the development of the BMRs shown in Figures 6 and 7 with the development one might expect from the random-walk plus solar differential rotation (2), in their early stages these BMRs were approximated by point doublets and regarded as sources of magnetic flux. (A point doublet consists of a pair of magnetic fluxes, having equal strength but opposite sign, located at points separated slightly from each other.) The locations of each of the two components of a doublet were taken to be the centers of sunspot area of leading and following magnetic polarity, respectively, within a day of the time of greatest total sunspot area. The doublet components of 15851 were located at (N23.25°, W50.50°) and (N20.75°, W57.50°) on August 14, 1964, at 8AM PST. This was a new-cycle group of the northern hemisphere with its leading flux of -9.9 SFU being 2.5° closer to the equator than its following flux of +9.9 SFU. The doublet components of 15852 were located at (N7.50°, E9.00°) and (N6.50°, E13.00°) on August 15, 1964, at 10AM PST. This was an old-cycle group of the northern hemisphere with its leading flux of +4.7 SFU being 1° further from the equator than its following flux of -4.7 SFU. The tilt of the doublet axis of this group is thus reversed from the usual situation, whereas the doublet axis of group 15851 is tilted normally (11).

Roberts (22) has devised a computer program to describe the distribution of magnetic flux on the solar surface resulting from the action of the random-walk and differential rotation on doublet sources. With the sources of groups 15851 and 15852, Roberts obtained distributions corresponding to the field patterns shown in the Z-photos of Figures 6 and 7. His results are shown in

Figures 8 and 9. Without considering Roberts' work in detail, we shall simply refer to the numbers plotted in Figures 8 and 9 as the magnetic fluxes in SFU located within squares defined by parallels of latitude and longitude 6° apart. This method of display is somewhat analogous to the concentration of magnetic flux at the boundaries of the supergranulation cells, the 6°-squares having roughly twice the diameter of the supergranulation cells, however. The random-walk step rate was taken to correspond to a ten-year decay time of an initial dipole field (T_0 = 20 years in reference (2)). Only fluxes of at least 0.1 SFU per square are included in Figures 8 and 9. A positive sign refers to a magnetic vector directed toward the observer, and a negative sign refers to a magnetic vector directed away from the observer. For technical reasons associated with the computer program, the longitudes in Figures 8 and 9 do not correspond precisely to the longitudes in Figures 6 and 7, a shift of a few degrees generally being required to obtain coincidence. Comparing Figures 6 and 7 with Figures 8 and 9 respectively, we see that the sizes, shapes, and total fluxes of the calculated and observed flux distributions are roughly the same. Furthermore, the flux distributions of groups 15851 and 15852 develop into quite different shapes, as one would expect from sources whose doublet axes are oppositely tilted. Since the calculation of flux distributions has not yet reached a completely satisfactory stage, the comparison of the measured flux distribution with the computer results must be regarded as very rough and tentative.

Figure 8

The flux distribution for Mount Wilson group 15851 on
September 6, 1964, as calculated by Roberts (22). The numbers
refer to fluxes in SFU, a positive flux corresponding to a magnetic
vector directed toward the observer and a negative flux corre-
sponding to a magnetic vector directed away from the observer.
Φ_l and Φ_f refer to the total flux of leading and following polarity
respectively. These fluxes are not equal because of an approxi-
mation made by Roberts in the computer solution for this flux
distribution.

$$\phi_L = -5.6 \; ; \; \phi_F = +4.3$$
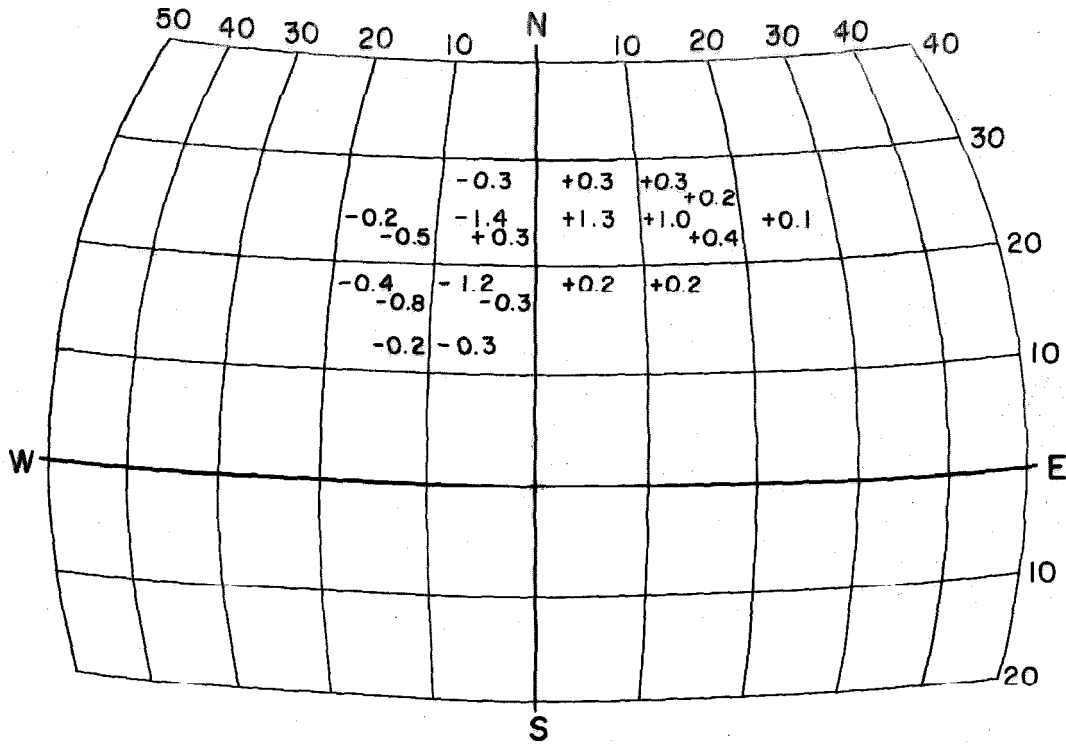
MWO 15851
9/6/64 20 O'CLOCK PST

Figure 8

Figure 9

(a)   The flux distribution for Mount Wilson group 15852 on
September 12, 1964, as calculated by Roberts (22).
The numbers refer to fluxes in SFU, a positive flux
corresponding to a magnetic vector directed toward
the observer and a negative flux corresponding to a
magnetic vector directed away from the observer. The
fluxes Φ_l and Φ_f refer to the total flux of leading and
following polarity.

(b)   The flux distribution for Mount Wilson group 15852 on
October 9, 1964, as calculated by Roberts. The
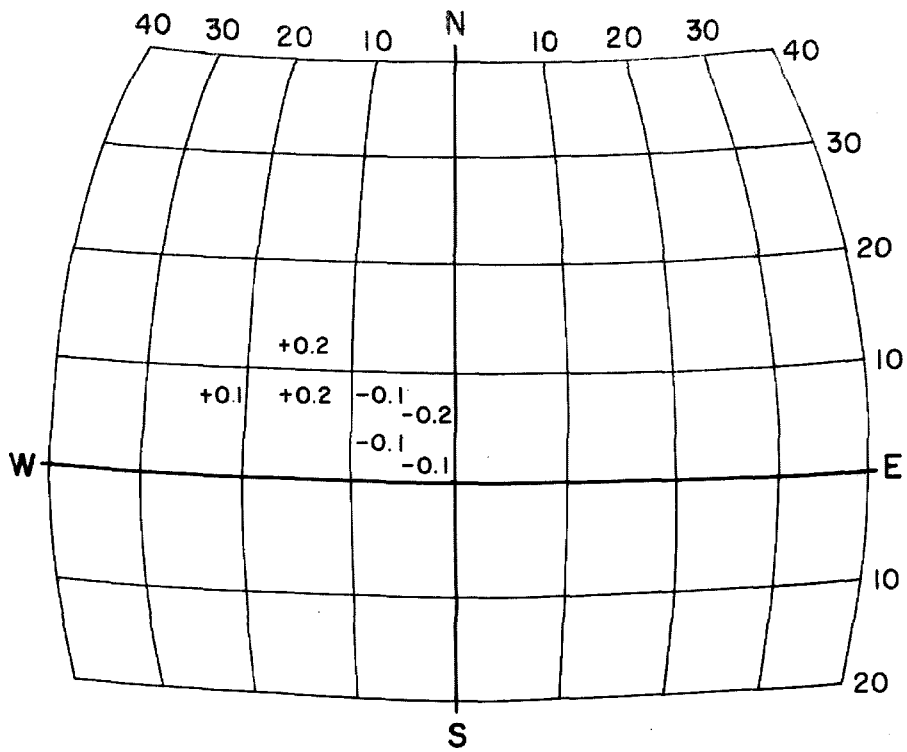numbers have the same meaning as in Figure 9(a).

$$\phi_L = +1.2 \, ; \, \phi_F = -1.1$$
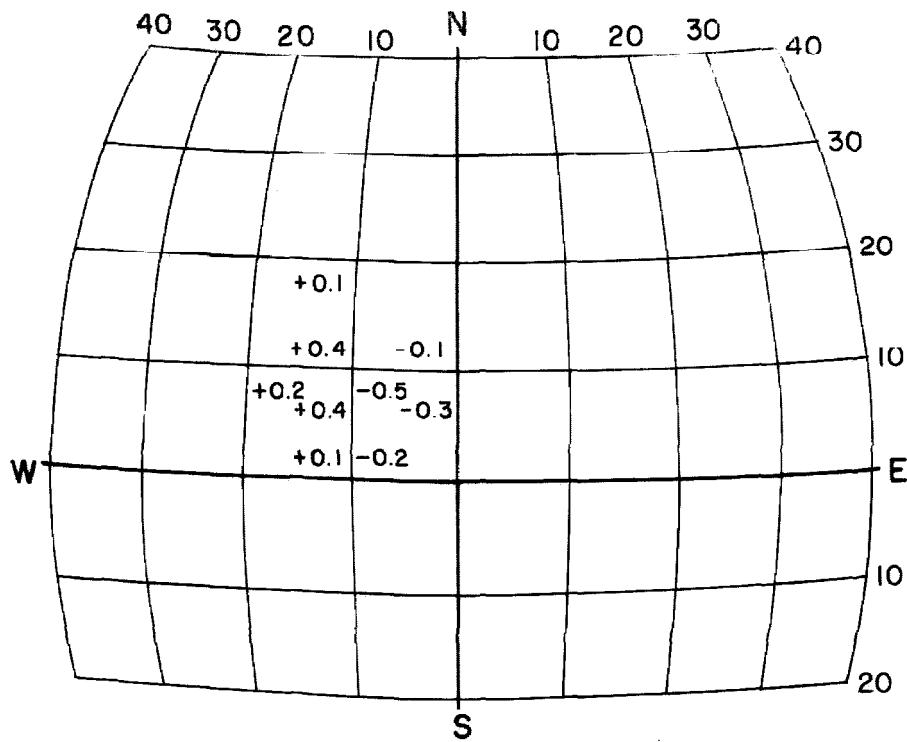
MWO 15852
9/12/64 16 O'CLOCK PST

Figure 9(a)

$$\phi_L = +0.5 \; ; \; \phi_F = -0.5$$

MWO 15852
10/9/64 17 O'CLOCK PST

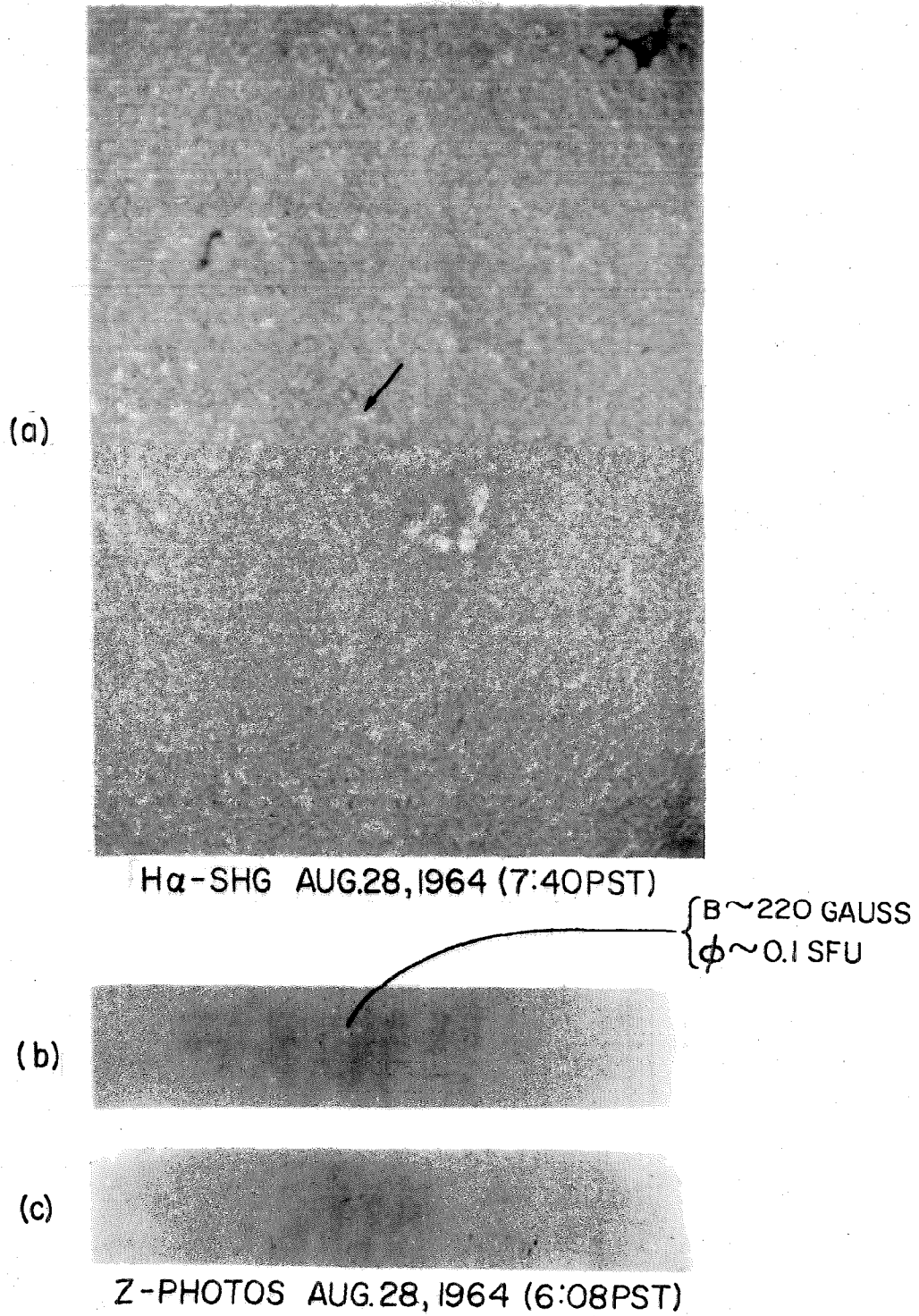Figure 9(b)

C. Small Scale Magnetic Fields

Z-photos show that in quiet regions of the solar surface magnetic flux is distributed in small bits and fragments, and, in the quietest regions, in tiny points less than 3000 km in diameter. Figures 10(b) and 10(c) show Z-photos of a region near the center of the solar disk on August 28, 1964, (Figure 10(c) corresponding to a time about 2 minutes later than the time of Figure 10(b)), and Figure 10(a) shows a spectroheliogram in the core of Hα showing this same area $1\frac{1}{2}$ hours later. The two Z-photos have opposite magnetic polarities. Two photos were included rather than one to aid in the identification of the very tiny magnetic features. (Note that the features in the Z-photo of Figure 10(c) do not appear as sharp as those of Figure 10(b). This was caused by a very slight misalignment of plates at the doubly-cancelled stage.) Note the very tiny light and dark points on the Z-photos, and note also that most of these points correspond to brighter-than-average features on the Hα-spectroheliogram (Hα-SHG), even though the SHG was exposed as much as $1\frac{1}{2}$ hours later. Typically, one finds fluxes of 0.05 - 0.1 SFU for these small magnetic features. Thus, one would expect the average magnetic fields of these relatively small features (a typical area $\sim 0.25 \times 10^{18} cm^2$) to be quite large

$$(B \sim \frac{\Phi}{A} \sim \frac{0.1 \times 10^{21} gauss\ cm^2}{0.25 \times 10^{18} cm^2} \sim 400\ gauss).$$

Figures 11 and 12 also show Z-photos of solar regions containing some small magnetic features. The magnetic fields of eight features, indicated in Figures 10, 11, and 12, were obtained from microphotometer tracings of the corresponding Zeeman plates using a microphotometer aperture small compared

Figure 10

(a) Spectroheliogram taken in the core of Hα about $1\frac{1}{2}$ hours after the Z-photos in Figure 10(b, c). The arrow indicates a brighter-than-average feature corresponding to the magnetic feature indicated in Figure 10(b).

(b) Z-photo in which lighter-than-average features indicate a magnetic field directed toward the observer (positive polarity) and darker-than-average features indicate a magnetic field directed away from the observer (negative polarity).

(c) Z-photo having the opposite polarity to that of Figure 10(b): darker-than-average features indicate positive fields and lighter-than-average features indicate negative fields. This Z-photo corresponds to a time about 2 minutes later than that of Figure 10(b). Two Z-photos were included rather than one to aid in the identification of the very tiny magnetic features that appear as lighter-than-average or darker-than-average points. The features in Figure 10(c) are not as sharp as those in Figure 10(b) because of a very slight misalignment of plates in the doubly-cancelled stage. Note that most of the very tiny magnetic features correspond to brighter-than-average features in the Hα-spectroheliogram even though it was taken about $1\frac{1}{2}$ hours after the Z-photos. In all three pictures, north is approximately toward the top of the page and east is to the right.

(a)

Hα-SHG AUG.28,1964 (7:40PST)

$\begin{cases} B \sim 220 \text{ GAUSS} \\ \phi \sim 0.1 \text{ SFU} \end{cases}$

(b)

(c)

Z-PHOTOS AUG.28,1964 (6:08PST)

8.2×10^4 KM

Figure 10

Figure 11

Z-photo showing some small magnetic features. Lighter-than-average features indicate a positive magnetic polarity (magnetic vector directed toward the observer), and darker-than-average features indicate a negative magnetic polarity (magnetic vector directed away from the observer). Features C and D are remnants of the BMR associated with MWO group 15852 (see Figure 7). North is approximately toward the top of the page and east is to the right.

Z – PHOTO

OCT. 9, 1964

8.2x10^4 KM
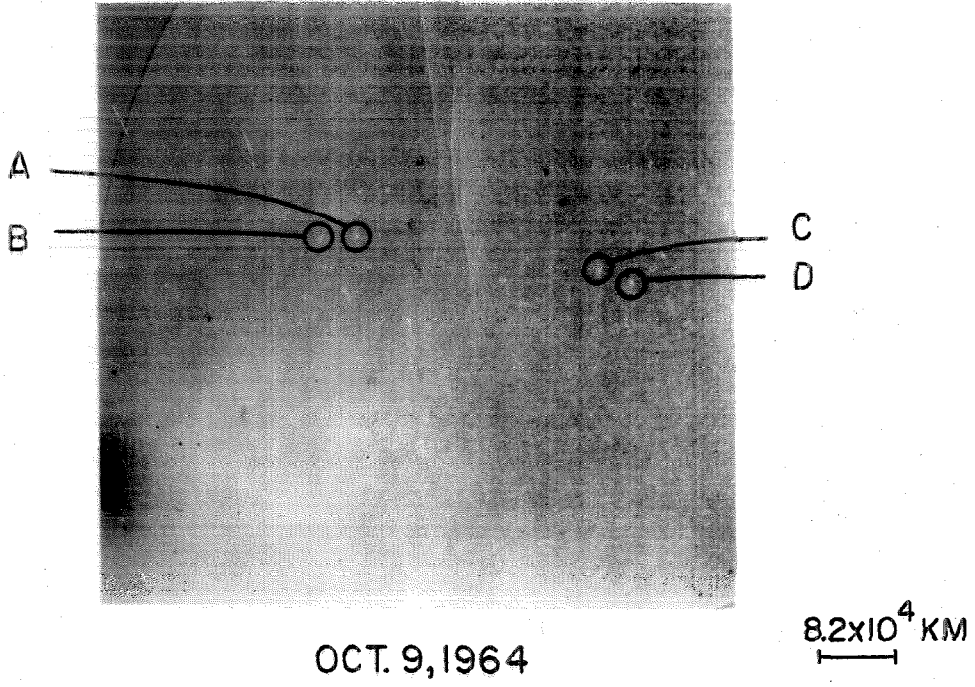
FEATURE	FLUX	FIELD	RANGE OF FIELD
A	0.1	220	130-350
B	0.05	390	300-490
C	0.2	290	230-350
D	0.2	480	390-570

Figure 11

Figure 12

The top photograph is a spectroheliogram taken near the solar disk center in the core of Hα. The other two photographs are Z-photos of the same region. In the Z-photos, lighter-than-average features indicate positive magnetic polarity (magnetic vector directed toward the observer) and darker-than-average features indicate negative polarity (magnetic vector directed away from the observer). North is approximately toward the top of the page, and east is to the right. Note the following:

1. In detail, wherever there are adjacent regions of opposite magnetic polarity, there are disk filaments in Hα. Note, especially that the three white dots of positive magnetic field nearly surrounded by field of negative polarity are encircled by a small absorbing feature in the Hα spectroheliogram.

2. The region in the photographs seems to contain four bipolar regions. Three of these are in the southern hemisphere, including the one with the large leading sunspot, and the other BMR is in the northern hemisphere. The region containing the large sunspot has apparently formed in another BMR just to the north of it, thus giving the impression of a single bipolar region.

3. No magnetic flux is indicated in the umbra of the large sunspot, although some flux is indicated in its penumbra.

4. Although it is not apparent from this figure, the following part of the BMR in the northern hemisphere is the westernmost limit of the large unipolar magnetic region (UMR) that was observed for many solar rotations in 1963. The BMR seems to have formed near the western end of the UMR and contributed additional flux of following (negative) polarity to it. The very bright and somewhat round magnetic feature in the leading part of this BMR corresponds to a sunspot.

5. Although it is not evident from the figure, sunspots are located in those features having 720 gauss or more.

70

Hα-SHG

Z-PHOTO
(FIELDS IN GAUSS)

720 —
720 —
720 —

230(I)
700(2)
600
660 (3)
1030
1100
1000
860

1.4 —
1.4 —

4.0 —

0.2
0.3
0.4
0.2
7.6

Z-PHOTO
(FLUXES IN SFU)

SEPT. 16, 1963

8.2×10^4 KM

FEATURE	FLUX	FIELD	RANGE OF FIELD
1	0.2	230	170-290
2	0.3	700	600-810
3	0.4	660	550-780

Figure 12

to the size of the features. Microphotometer tracings of two of these eight features are shown in Figures 13 and 14, respectively. Two tracings were made for each of these features, one from a plate on which the feature appeared lighter-than-average, and the other from a plate on which this same feature appeared darker-than-average.

Next, as illustrations, we shall derive the magnetic fields of these two features from the tracings of Figures 13 and 14. First, consider the tracings shown in Figure 13. We shall obtain the field from these tracings in two ways:

1. From Figure 13(a), we find $T = 0.95 {}^{+0.15}_{-0.05}$ and $T_0 = 0.70 \pm 0.10$. The expanded line profile yields

$$\frac{d \log_{10} T_{orig}(\lambda)}{d\lambda} = 4.9 \text{ A}^{-1} \text{ corresponding to}$$

$B_{\parallel} = 1470 \log_{10}(\frac{T}{T_0})$ gauss. We form three possible

values of $\frac{T}{T_0}$: $\frac{0.95}{0.70} = 1.36, \frac{1.1}{0.6} = 1.84, \frac{0.9}{0.8} = 1.12$

from which we obtain $B_{\parallel} = 190$ gauss, 380 gauss, 70 gauss. Proceeding similarly, we find from Figure 13(b) that $T = 0.4 \pm 0.05$ and $T_0 = 0.6 \pm 0.1$. Again we form three

values of $\frac{T}{T_0}$: $\frac{0.4}{0.6} = 0.67, \frac{0.35}{0.70} = 0.50, \frac{0.45}{0.5} = 0.90$

corresponding to $B_{\parallel} = 250$ gauss, 440 gauss, 70 gauss.

2. The value $\frac{d \log_{10} T_{orig}(\lambda)}{d\lambda} = 4.9 \text{ A}^{-1}$ can also be used to

obtain $B_{\parallel} = 640 \left\langle \frac{\Delta T}{T_0} \right\rangle_{GM}$ gauss. From the above, we have

three values of $\frac{\Delta T}{T_0}$ for Figure 13(a): 0.36, 0.84, 0.12,

Figure 13

(a) Microphotometer tracing of the transmission on the Z-photo shown in Figure 10(c). The feature 1 refers to the feature indicated in Figure 10, and although this feature was lighter-than-average on the plate microphotometered, it appears darker-than-average in Figure 10(c).

(b) Microphotometer tracing of the transmission on the Z-photo shown in Figure 10(b). Although the feature 1 was darker-than-average on the plate microphotometered, it appears lighter-than-average in Figure 10(b).
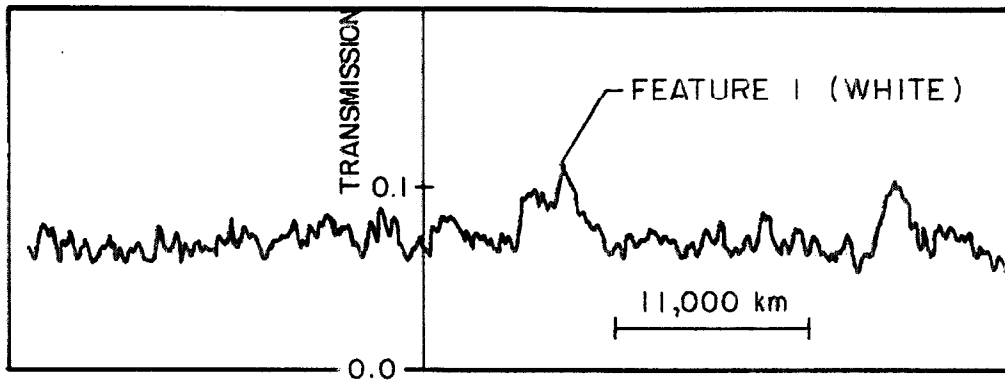
(a)
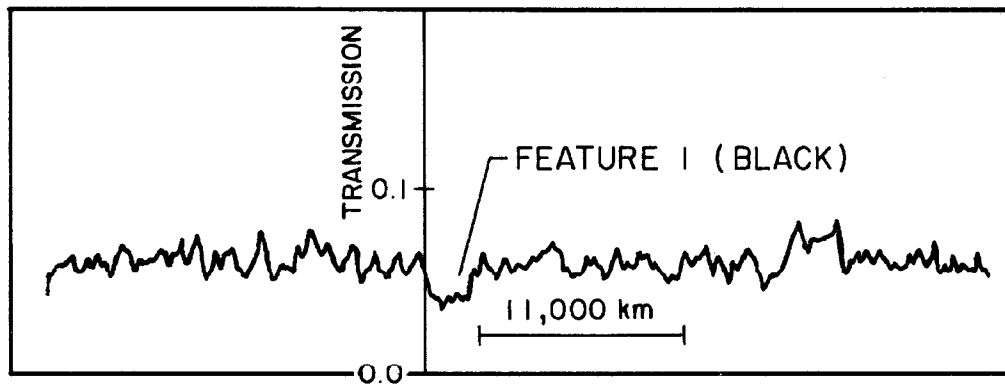
(b)

Figure 13

Figure 14

(a)   Microphotometer tracing of the transmission on the Z-photo
shown in Figure 12. Although feature 2 was lighter-than-
average on the plate microphotometered, it appears darker-
than-average in Figure 12.

(b)   Microphotometer tracing of the transmission on the Z-photo
having transmission reciprocal to that of the one shown in
Figure 12. Feature 2 was darker-than-average on the plate
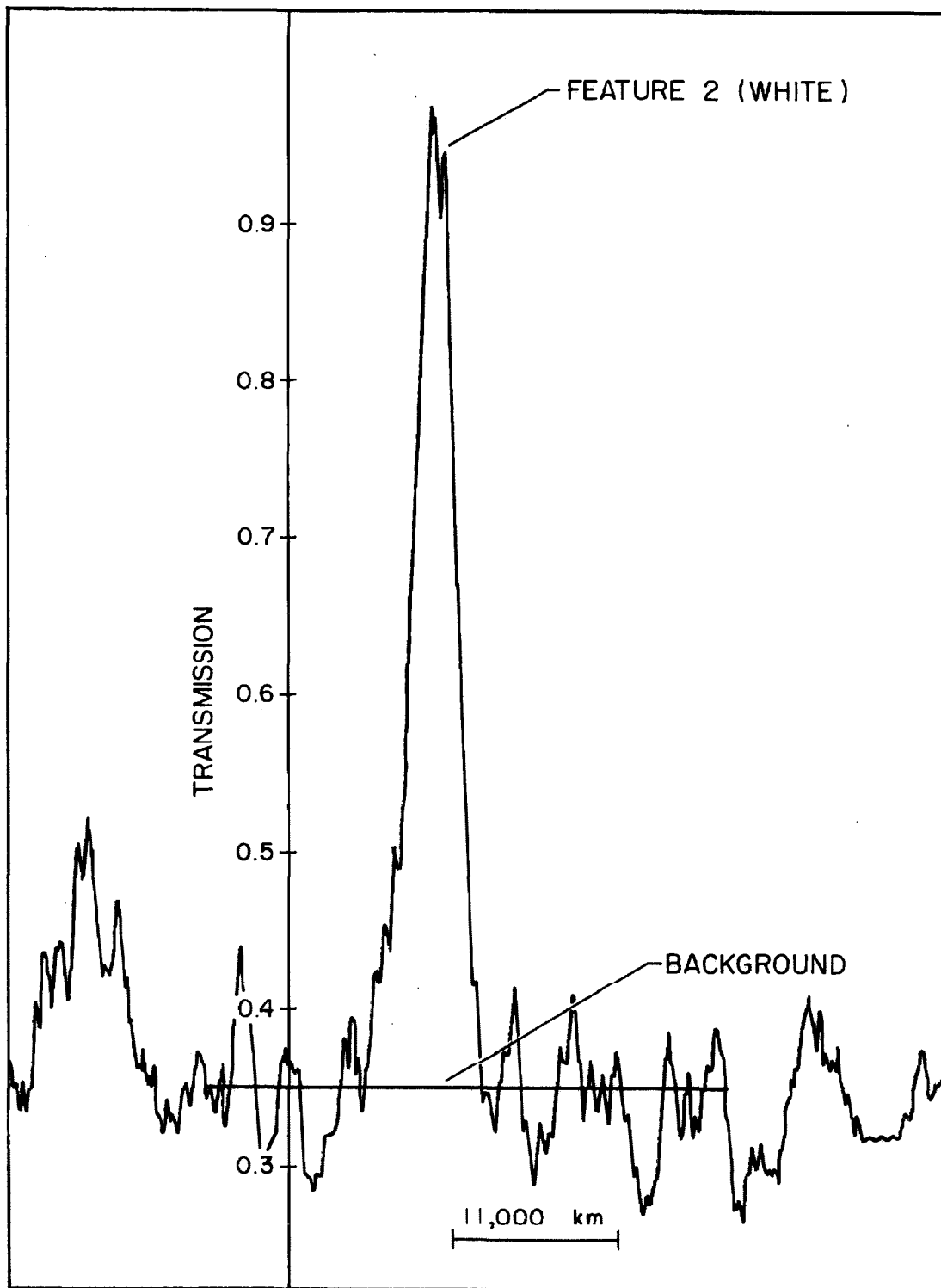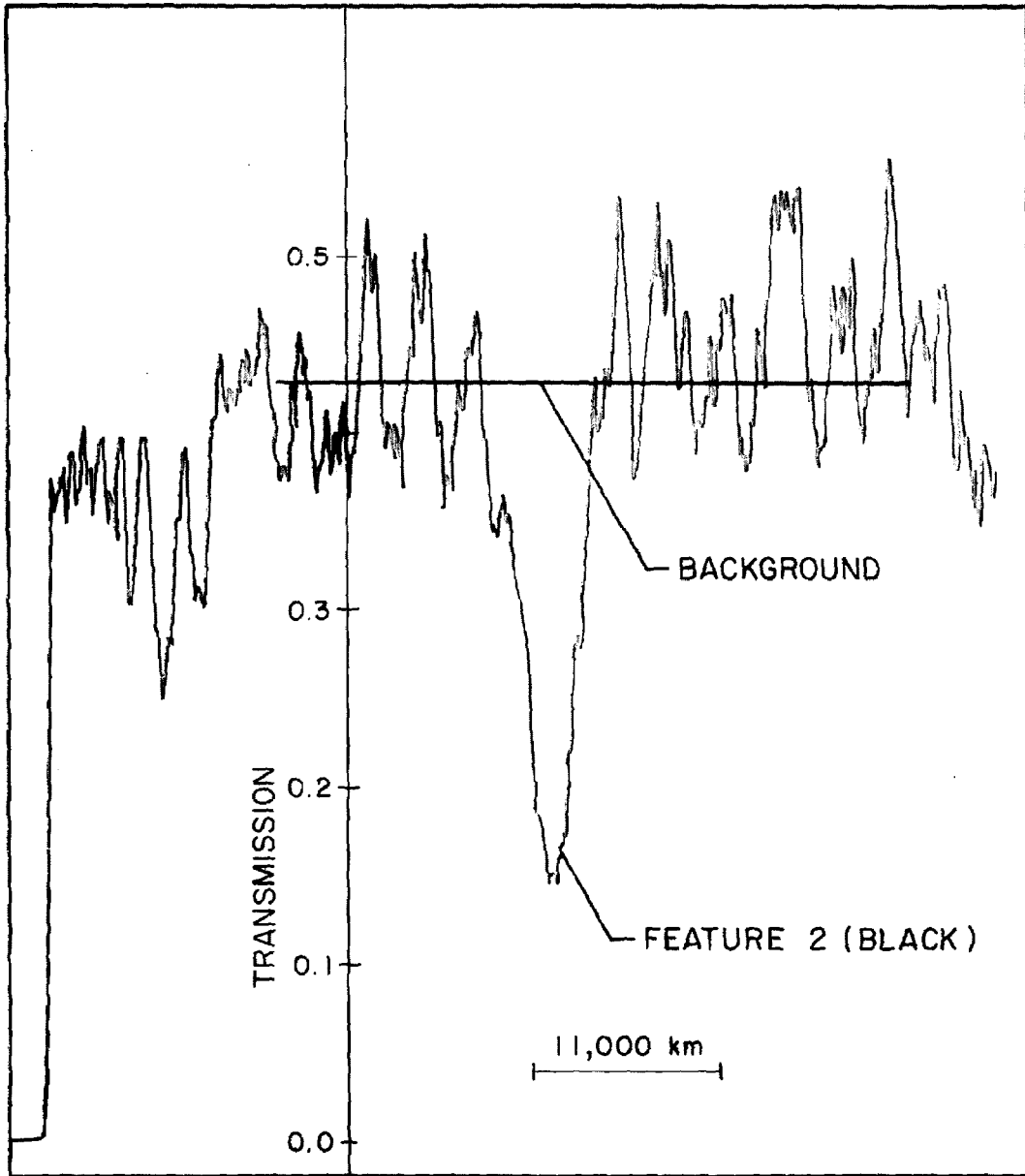microphotometered.

Figure 14(a)

Figure 14(b)

and three values of $\frac{\Delta T}{T_0}$ for Figure 13(b): -0.33, -0.50,

-0.10. From these we obtain three values of

$\left\langle \frac{\Delta T}{T_0} \right\rangle_{GM}$: 0.34, 0.65, 0.11 corresponding to

$B_{||}$ = 220 gauss, 420 gauss, 70 gauss.

Second, consider the tracings of Figures 14(a) and 14(b). Again we shall obtain the field in two ways:

1. From Figure 14(a) we find T = 9.65 ± 0.05 and

   T_0 = 3.5 ± 0.5. The expanded line profile yields

   $\frac{d \log_{10} T_{orig}(\lambda)}{d\lambda} = 4.8 \ A^{-1}$ corresponding to

   $B_{||}$ = 1500 $\log_{10} \left(\frac{T}{T_0} \right)$ gauss. We form three possible

   values of $\frac{T}{T_0}$: $\frac{9.65}{3.5}$ = 2.76, $\frac{9.70}{3.0}$ = 3.23, $\frac{9.60}{4.0}$ = 2.40

   from which we obtain $B_{||}$ = 660 gauss, 760 gauss, 670 gauss.
   Proceeding similarly we find from Figure 14(b) that T = 1.5
   and T_0 = 4.3 ± 0.5. Again we form three values of

   $\frac{T}{T_0}$: $\frac{1.5}{4.3}$ = 0.35, $\frac{1.5}{4.8}$ = 0.31, $\frac{1.5}{3.8}$ = 0.40 corresponding to

   $B_{||}$ = 690 gauss, 750 gauss, 600 gauss.

2. The value $\frac{d \log_{10} T_{orig}(\lambda)}{d\lambda} = 4.8 \ A^{-1}$ also corresponds to

   $B_{||}$ = 650 $\left\langle \frac{\Delta T}{T_0} \right\rangle_{GM}$ gauss. From the above, we have the

   values of $\frac{\Delta T}{T_0}$: 1.76, 2.23, 1.40 for Figure 14(a), and the

   values of $\frac{\Delta T}{T_0}$: -0.65, -0.69, -0.60 for Figure 14(b).

From these we obtain the values of $\left\langle \frac{\Delta T}{T_0} \right\rangle_{GM}$: 1.07, 1.24, 0.92, corresponding to $B_{\parallel}$ = 700 gauss, 810 gauss, 600 gauss, respectively.

Table 5 summarizes the magnetic field measurements of these eight features. The first column contains the dates on which the Z-photos were taken. The second column identifies the features on these photos. The third column contains the magnetic fluxes in SFU obtained by the usual method described in Part II of this thesis. The fourth column contains the magnetic fields in gauss obtained from microphotometer tracings. The fifth column contains upper and lower limits of the field that one might obtain from different interpretations of the microphotometer tracings. Table 5 shows that magnetic fields of a few hundred gauss are not at all uncommon for these small magnetic features. We shall interpret this result in Part IV of this thesis.

D. Magnetic Flux on the Polar Caps of the Sun as a Function of
    Time During the Period 1905-1964.

The numbers of north and south polar faculae have been counted for the period 1905-1964. The chief results have already been published (3), and are reprinted here in Appendix III for convenient reference. Next, we shall consider some further results of counting polar faculae, and then describe a method of calibrating the number of polar faculae in terms of magnetic flux normal to the solar surface.

TABLE 5

date	feature	flux*(SFU)	field (gauss)	Possible range of field (in gauss)
8/28/64	1	0.1	220	70-420
10/9/64	A	0.1	220	130-350
	B	0.05	390	300-490
	C	0.2	290	230-350
	D	0.2	480	390-570
9/16/63	1	0.2	230	170-290
	2	0.3	700	600-810
	3	0.4	660	550-780

* The accuracy of these flux measurements is roughly
$\pm$ (0.05 - 0.10) SFU.

Figure 3 of Appendix III shows the numbers of north and south polar faculae plotted versus time for the period 1905-1964. The numbers of north polar faculae were obtained for each year from photographic plates taken during the August 15 - September 15 interval when the Earth has its northernmost heliographic latitude. Similarly, the numbers of south polar faculae were obtained for each year from photographic plates taken during the February 15 - March 15 interval when the Earth has its southernmost heliographic latitude. The numbers of north and south polar faculae were also obtained from photographic plates taken during the February 15 - March 15 and August 15 - September 15 intervals when the respective poles are least visible from the Earth. These numbers of north and south polar faculae have been plotted versus time for the period 1905-1964, and are shown in Figure 15. Comparison between Figure 3 of Appendix III and Figure 15 shows that the amplitudes of the polar faculae curves obtained from plates taken during the favorable intervals are approximately 2.0 to 2.5 times the amplitudes of the polar faculae curves obtained from plates taken during the unfavorable intervals. (This is what one would expect if the polar faculae were distributed roughly uniformly over caps having half-angles between 30° and 40°.) Therefore, to obtain the number of polar faculae over an entire polar cap, the number obtained from plates taken during the corresponding favorable interval must be multiplied by approximately 1.5. Hence, if the scale of the numbers of polar faculae in Figure 3 of Appendix III were multiplied by 1.5, the curves would describe the number of polar faculae covering the entire polar caps as a function of time.

Figure 15

Numbers of north and south polar faculae counted for each year in the period 1905-1964 during the one-month interval when the respective polar region was least favorably oriented with respect to the Earth. (Note that the scales for the numbers of north and south polar faculae are not the same.) Compare this figure with Figure 3 of Appendix III which shows similar measurements obtained when the respective polar regions were most favorably oriented with respect to the Earth.
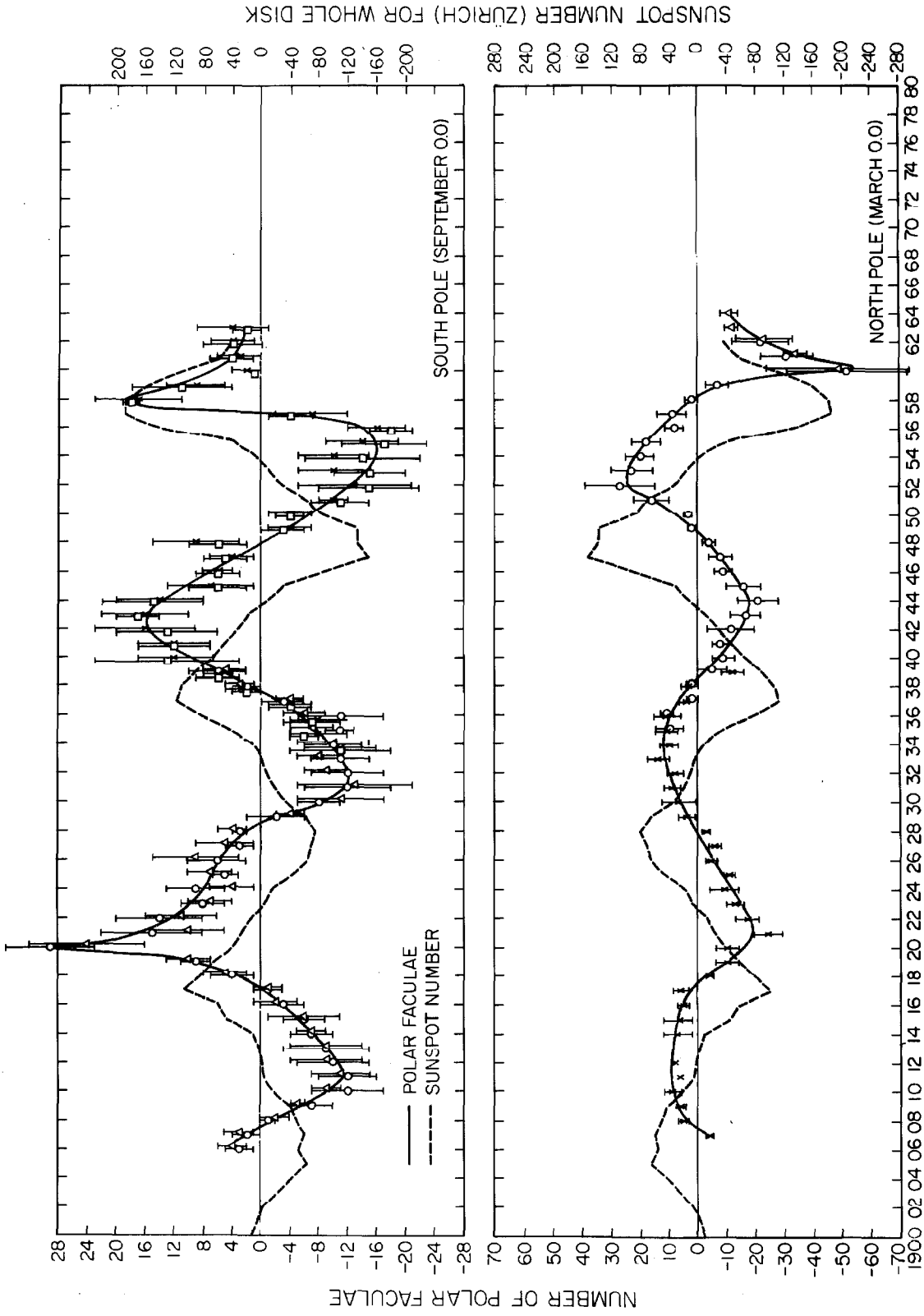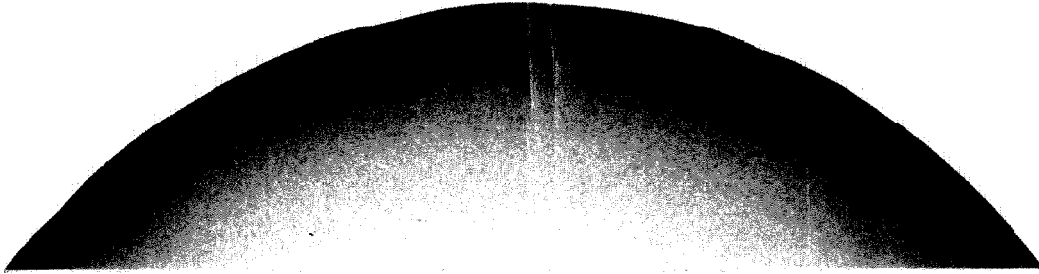
Figure 15

Figure 16 shows the portions of direct photographs of the
solar disk north of $40^{\circ}N$ latitude for August 31, 1952;
September 11, 1948; August 30, 1920. These photographs were
obtained at the 60-foot tower on Mount Wilson, and are repre-
sentative of the plates used for counting polar faculae. Figures
16(a) and 16(c) show that there are considerable numbers of polar
faculae on the 1952 and 1920 photographs, but Figure 16(b) shows
none at all on the 1948 photograph. In each of these pictures,
north is directly toward the top of the page and east is to the right.
In the 1952 and 1920 photographs, the polar faculae cover caps
having half-angles of roughly 35°. In the 1920 photograph, the
mark west of the north pole is an improperly-placed polemarker.
This mistake was discovered by noticing that the polar faculae do
not center about the polemarker. In the process of looking at
plates, several cases were found in which the polar faculae did
not center about the polemarker. In every such case, when the
position of the polemarker was checked, it was found to be im-
properly placed, the correct position always being in the midst
of the polar faculae. This is consistent with Babcock's finding (23)
in 1952-1953 of "no evidence of any persistent obliquity between the
magnetic and rotational axes" of the sun, and extends this finding
to the very much longer period 1905-1964.

A way has been found to calibrate polar faculae in terms of
magnetic flux. This enables one to use the polar faculae curves
of Figure 3 of Appendix III to obtain the total magnetic fluxes on
the north and south polar caps, respectively, as a function of time
during the period 1905-1964. The calibration was achieved as
follows: The heliographic position was noted for a region of
equatorial faculae located near the east limb of the sun, the faculae

Figure 16

Portions of direct photographs of the solar disk north of
40^ON latitude for August 31, 1952; September 11, 1948;
August 30, 1920. Note the considerable number of polar faculae
in the upper and lower pictures, and the striking lack of such
brighter-than-average features in the middle photograph. In
each picture north is toward the top of the page and east is to
the right. The mark west of the north pole in the lower picture
is an improperly-placed polemarker, as one might expect since
the polar faculae are not centered about it.

(a)

August 31, 1952

(b)
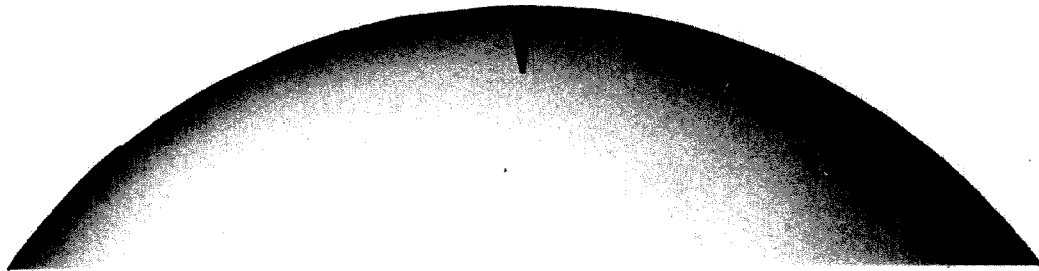
September 11, 1948

(c)

August 30, 1920

Figure 16

having approximately the same size and intensity on a Mount Wilson direct photograph as polar faculae on the same photograph. This region was identified on a spectroheliogram taken in the core of Hα within a few hours of the time of the direct photograph, and was followed daily on Hα spectroheliograms until it rotated into the disk center. (Individual features generally could no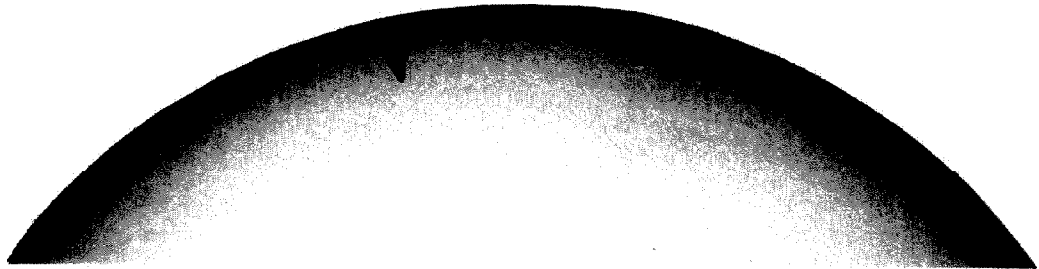t be followed from the limb to disk center because their lifetimes were less than two days.) Then the Hα spectroheliogram was compared with a Z-photo taken within roughly an hour of the time of the spectroheliogram, and features corresponding to Hα faculae were identified on the Z-photo. These features had a fragmentary appearance on both the spectroheliogram and the Z-photo. Their fluxes were measured, and an average flux per fragment estimated. Then, assuming that the average polar facula has the same flux as the average equatorial facula of similar size and intensity, the magnetic flux on a polar cap was obtained by multiplying the number of polar faculae on that cap by the average flux per fragment. (We have already seen that the ordinates of the graphs in Figure 3 of Appendix III must be multiplied by 1.5 to give the numbers of polar faculae on the entire caps.)

The above procedure was carried out for two equatorial regions. The first region consisted of the following part of an old BMR moving in from the east limb on September 2, 1964, and reaching the disk center around September 7. Although this was the second disk appearance of the BMR associated with Mount Wilson sunspot group 15851 (see Figure 6) in Part III (B) a small sunspot remained in the leading part until September 6, thus giving rise to the Mount Wilson number 15853 associated with the second appearance of this BMR. Despite the fact that individual faculae in

the following part of this BMR generally could not be traced on Hα spectroheliograms from their positions on September 2 to their positions on September 7, statistically these faculae formed a pattern which could be traced from September 2 to September 7. On the average, the faculae near the west end of this following region tended to be larger and brighter than the faculae near the east end of this following region. The faculae near the east end corresponded to the smaller and fainter of the polar faculae, whereas some of the Hα faculae near the west end corresponded to white light faculae generally larger and brighter than most polar faculae. Magnetic fluxes of several features near the west end, middle, and east end of this region were measured on September 6 and September 7. The second equatorial region consisted of an old BMR moving in from the east limb on September 7, 1964, and reaching the disk center about September 12, 1964. This BMR corresponds to Mount Wilson sunspot group 15852, and is shown on September 12 in Figure 7 in Part III (B). On September 7, most equatorial faculae of this BMR appeared to have roughly the same size and brightness as typical polar faculae. However, one equatorial facula was considerably larger and brighter than the largest and brightest of the polar faculae. The magnetic fluxes for this region were measured for September 12, 1964.

Table 6 shows the measured fluxes for the two equatorial regions described above. The first column identifies the equatorial regions. The second column contains the dates for which magnetic fluxes were measured. The third column contains the fluxes in SFU of various magnetic features, classified according to location in the respective equatorial regions. The fourth column contains the average flux per feature, evaluated for different parts of the

TABLE 6

region	date	fluxes		average flux
following part of 15851	9/6/64	east end	0.2	0.2
		middle	0.2	
			0.1	
			0.1	0.13
		west end	0.6	
			0.2	0.4
following part of 15851	9/7/64	east end	0.1	
			0.2	0.15
		middle	0.6	
			0.0	
			0.1	
			0.1	
			0.0	0.16
		west end	0.1	
			0.0	
			0.8	
			0.4	0.32
15852	9/12/64		0.1	
			0.2	
			0.1	
		leader	0.9	
			0.3	
			0.1	
			0.2	
			0.2	0.26
		follower	0.3	
			0.1	
			0.1	
			0.3	
			0.2	
			0.2	0.20

two equatorial regions measured. Table 6 shows that the average flux per magnetic feature near the middle and east end of the following part of 15851 was approximately 0.1 - 0.2 SFU, whereas the average flux per feature near the west end was 0.3 - 0.4 SFU. The average flux per feature in the BMR corresponding to group 15852 was 0.2 SFU in both the leading and following parts. The especially large value of 0.9 SFU was obtained for a magnetic feature in the leading part of 15852. This probably corresponds to the especially large and bright faculus seen on September 7 near the east limb. In conclusion, we shall adopt 0.2 SFU as the magnetic flux corresponding to the average polar facula, with 0.1 SFU and 0.3 - 0.4 SFU corresponding to the smaller, fainter polar faculae and the larger, brighter polar faculae, respectively.

Now, let us use the above results to obtain the magnetic flux on the polar caps as a function of time during the period 1905-1964. Referring to Figure 3 of Appendix III, the average amplitude of the polar faculae curves is roughly 40. Multiplying by 1.5, we obtain 60 as the number of faculae over an entire polar cap when the polar field has its relatively largest flux. Using 0.2 SFU per polar facula, we find 60 x 0.2 SFU = 12 SFU as the approximate amplitude of the corresponding polar-magnetic-flux versus time curves. However, Figure 3 of Appendix III shows that the polar faculae maxima are not all the same. In 1912, the numbers of north and south polar faculae were both about 20 corresponding to 20 x 1.5 x 0.2 SFU = 6 SFU, whereas in 1961 the number of north polar faculae was about 70 corresponding to 70 x 1.5 x 0.2 SFU = 21 SFU. In general, the ordinates of Figure 3 of Appendix III may be converted to total magnetic flux on the respective polar caps by multiplying the number of polar faculae counted by

1.5 x 0.2 SFU = 0.3 SFU. This flux refers, not to the line-of-sight component, but to the component normal to the solar surface.

Finally, note that we have generally assumed that for a given pole of the sun all of the polar faculae correspond to magnetic features having the same magnetic polarity. This seems justified for two reasons: First, we know that in the sunspot belts, contiguous regions of opposite magnetic polarity seem always to show Hα disk filaments (or prominences on the limb). If the polar regions contained mixed polarities, one would expect to find such Hα filaments and prominences here also. These Hα features are found at the poles only near the time of sunspot maximum when the numbers of polar faculae are very small or zero. Second, solar magnetograms obtained by Babcock show that near the time of the last sunspot minimum (1953-54) when there were considerable numbers of polar faculae each polar region contained relatively strong fields of a single polarity, whereas near the last sunspot maximum each polar region occasionally contained fields of both magnetic polarities. We shall see later than special care must be taken in the interpretation of polar magnetograms obtained near sunspot maximum.

IV. Discussion

We have considered several different aspects of solar magnetism at some length. Now we shall examine our results to see what has been learned and what conclusions may be drawn about the sun. In section A we shall review this research and summarize its chief results. In section B we shall analyze these results to see what we have learned. In section C we shall attempt to draw a conclusion.

A. Review and Summary of Measurements

1. Magnetic Fluxes Associated with Sunspot Groups

Magnetic fluxes associated with sunspot groups were measured using a photographic technique. Fluxes in the umbras of sunspots were supplemented by fluxes calculated from the Mount Wilson magnetic observations of sunspots whenever these observations were available. Whenever an appreciable imbalance between fluxes of positive and negative polarity was obtained photographically, a corresponding imbalance of sunspot umbral flux was obtained. The sunspot flux imbalance was always in the direction to account for the photographic imbalance, but, especially when small sunspots were involved, the spot flux imbalance was not always large enough to account for the photographic imbalance. We shall see later that this may be the result of a systematic error in the measurement of the fields in small sunspots in the Mount Wilson observations.

The fluxes associated with sunspot groups varied considerably from group to group. A flux of 0.2 SFU was measured

for a small BMR in which sunspots were never observed at Mount Wilson. Typical spot groups during the summer of 1964 had fluxes ranging from 1 to 5 SFU. The sunspots in these groups generally were very small, without penumbras, and did not last more than a week. A moderate-sized sunspot group having a characteristic leading spot with penumbra was measured in the autumn of 1963 and a flux of approximately 12 SFU obtained. A very large and active γ-type sunspot group with considerable penumbras was measured and found to have 20-40 SFU. These measurements were compared with three flux measurements of Bumba (15) who obtained values ranging from 14 SFU to more than 50 SFU for very large sunspot groups.

The flux of a given BMR generally increased to a maximum value in a few days or less and then slowly declined. A source flux, Φ, was defined as the average of the absolute values of the total fluxes of leading and following polarity in a given BMR at the time when this average was greatest. Since the leading and following fluxes balanced within measurement accuracy, the source flux, Φ, can be interpreted as the amount of flux emanating from one part of a BMR and returning to the other part. To describe the variation of source flux with sunspot group size more precisely, a parameter of spot group size, A_m, was defined. A_m is the area of the solar surface covered by all the sunspots of a group (umbras plus penumbras of both leading and following parts) at the time when this area is largest. The source fluxes were found to satisfy $\Phi = 1.2\,A_m$ within measurement accuracy, where Φ is in SFU and A_m is in units of $10^{18}\,cm^2$. When values of A_m were measured for the spot groups Bumba studied, it was found that his fluxes also satisfy $\Phi = 1.2\,A_m$.

2. The Development of BMRs

During the summer and autumn of 1964 the magnetic fields of BMRs were observed daily from their birth until they were no longer detectable by the photographic technique. The time during which a BMR remained detectable depended on the source flux of the BMR. The small BMR with a source flux of 0.2 SFU lasted only a few days, whereas BMRs with source fluxes of 5-10 SFU were detectable after two solar rotations.

Two BMRs were traced for more than a solar rotation, and one of these was detectable after two solar rotations. In each of these BMRs, the sunspots disappeared after a few weeks. (It is difficult to say how long the spots lasted because both groups passed out of sight around the west limb of the sun. At this time, all that remained of the spots of one BMR was a small leading spot. The spot activity of the other group apparently had reached maximum just before the group passed around the west limb. On their returns, no spot was seen in the first BMR and only a small leading spot was visible in the second BMR. This spot disappeared a few days after the return of the BMR around the east limb.) A comparison of the development of these two BMRs is particularly interesting because the axes of their corresponding spot groups were tilted in opposite directions. One group was a new-cycle group at 22^ON latitude, and had a source flux of approximately 10 SFU. The sunspots of leading polarity were located about 2.5 degrees closer to the equator than the spots of following polarity so that the spot group axis was tilted in the usual direction (11). The other group was an old-cycle group at 7^ON latitude, and had a source flux of about 5 SFU. The sunspots of leading polarity were located about 1 degree farther from the equator than the spots of

following polarity so that the tilt of the spot group axis was reversed from the usual direction. The new-cycle BMR developed with its leading part dominating at lower latitudes and its following part, trailing eastward in a manner characteristic of differential rotation, dominating at higher latitudes. The old-cycle BMR, with the reverse-tilted spot axis, developed in a different pattern, its leading part dominating at higher latitudes. Both of these patterns of development are roughly what one would expect if the random-walk plus differential rotation were the dominant means of flux transport.

Roberts (22), using a preliminary program he has devised for the development of BMRs by the random-walk plus differential rotation, computed the development of these two BMRs from the measured positions and strengths of their sources. The observed sizes, shapes, and total fluxes of these BMRs after more than a solar rotation were roughly what Roberts calculated. We consider this result tentative due both to the preliminary state of Roberts' program and to the uncertainties in the selection of heliographic positions of the sources.

As the BMRs developed, the fluxes were distributed over progressively larger areas. The flux density did not decrease smoothly from the vicinity of the source to the outer limit of detectable flux. Rather, the flux was distributed in progressively smaller bits and fragments. In the last detectable stages of the BMRs, only small bits and points of flux remained. These final concentrations of flux were less than 5000 km in diameter and often smaller down to the limit of the photographic resolution of roughly 1000 km. Next, we shall review our study of these small-scale features.

3. Small-Scale Magnetic Fields

It was observed that, as BMRs develop, their fluxes are distributed in bits and fragments of progressively smaller size until finally they escape detection below our photographic threshold. Measurements for eight small features yielded fluxes ranging from 0.05 SFU for very small points less than 3000 km in diameter to 0.4 SFU for rather large networklike fragments. The corresponding magnetic fields ranged from 200 gauss for the points to 700 gauss for the large fragments. Even allowing for an error of as much as a factor or two, these fields were considerably larger than had been anticipated. Field measurements were then made to see how much stronger non-spot fields might be in active regions. The magnetic fields, even in active regions, never were greater than about 700 gauss outside sunspots. Fields of 800-1500 gauss were found in small sunspots. To the limit of the spatial resolution of the photographic technique, sunspot magnetic fields, even in the smallest spots, seem to be greater than the largest non-spot fields, although a systematic study was not undertaken. Sunspots with fields much greater than 1500 gauss generally were so dark that they appeared underexposed on our plates, thus giving no fields at all. Comparison of our measured spot fields with a few Mount Wilson magnetic observations showed agreement within 30-50% for Mount Wilson measurements greater than about 800 gauss. However, the Mount Wilson measurements of less than 700 gauss for the small sunspots seem appreciably smaller than our measurements. Allowing at worst a factor of two for the somewhat uncertain photographic error in our measurements, Mount Wilson spot fields less than 350 gauss may be attributed to poor seeing conditions, the

difficulty of holding small sunspots on the entrance slit at the
150-foot tower, and the difficulty of distinguishing differences
of magnetic field for sunspot fields as small as 350 gauss. Further
study of this discrepancy is surely necessary.

4. Magnetic Flux at the Poles of the Sun

The polar faculae relations (3) and Appendix III were
calibrated to give magnetic flux in the polar regions of the sun as
a function of time during the period 1905-1964. The calibration
was achieved statistically by measuring magnetic fluxes associated
with equatorial faculae of size and brightness similar to that of
polar faculae. An average flux of 0.2 SFU per measured equatorial
facula was obtained. To account for the polar faculae on the far
side of the sun that are not seen and therefore not included in the
polar faculae relations (3) and Appendix III, for each hemisphere
polar faculae were counted during intervals when the sun's axis
was most favorably and least favorably inclined with respect to the
earth. The amplitudes of polar faculae curves obtained from plates
taken during the favorable intervals were roughly twice the ampli-
tudes obtained from plates taken during the unfavorable intervals.
This corresponds to a correction factor of 1.5. One also obtains a
correction factor of 1.5 from purely geometrical considerations
assuming that during polar faculae maxima the faculae are distri-
buted uniformly over caps of half-angles between 30 and 40 degrees.
This is consistent with our observations that during polar faculae
maxima the faculae were distributed symmetrically about the
respective poles in caps of 30-40 degrees in half-angle. We thus
obtained a calibration factor of 1.5 x 0.2 SFU = 0.3 SFU per visible
polar facula.

The fluxes vary cyclicly with time approximately 90° out of phase with the variation of the sunspot number for the whole solar disk with time during the same 1905-1964 period (provided the sunspot number is given a polarity corresponding to the magnetic polarity of the following sunspots of the relevant hemisphere). The maxima of the polar fluxes vary considerably from cycle to cycle (just as the maxima of the sunspot number vary considerably from cycle to cycle), maximum fluxes ranging from 6 SFU to 21 SFU with 12 SFU being a typical maximum polar flux during 1905-1964. One may obtain the detailed variation by multiplying the scale of polar faculae in Figure 3 of Appendix III by 0.3 SFU per visible polar facula.

B. Analysis of the Results

In this section we shall examine our results to see what we now know that we did not know before, and to see how this new knowledge may be used to increase our understanding of the sun.

First, we know that during the period 1905-1964 the numbers of north and south polar faculae varied cyclicly with time about 90° out of phase with the variation of the sunspot number for the whole solar disk with time, provided the sunspot number is given a polarity corresponding to the magnetic polarity of the following sunspots of the relevant hemisphere. We have interpreted this as a measure of the time variation of the polar fields, and have noted that this variation is generally consistent with the supposition that sunspot groups provide sources of magnetic flux that is carried to the poles in a few years' time by means of the random-walk process associated with the convective supergranulation (2, 3, 4).

However, we also know that this cyclic variation is not regular. Not only do the maxima of the numbers of north and south polar faculae vary from cycle to cycle (just as the maxima of the sunspot number vary from cycle to cycle), but the numbers of faculae occasionally deviate from their general pattern of variation. For example, after increasing in 1940 the number of north polar faculae decreased in 1941 and 1942 before increasing again in 1943 (see Figures 1 and 3 of Appendix III). A second example is the rapid decrease in the number of south polar faculae in 1960 and 1961 and their continuing low number even during the present (1964) minimum of sunspot activity. The measurements of the numbers of north and south polar faculae are sufficiently accurate and reproducible (see Figures 1 and 3 of Appendix III) that these departures from a regular cyclic variation surely reflect the behavior of the polar fields of the sun. These deviations thus provide a means to test the random-walk hypothesis better than has heretofore been possible. If the random-walk plus differential rotation is the dominant means of flux transport on the solar surface, and if bipolar magnetic regions are the sources of flux, then one would expect this mechanism to account for the variation of polar faculae maxima from cycle to cycle, the decrease in the number of north polar faculae in 1941 and 1942, and the rapid decrease in the number of south polar faculae since 1959. In order to facilitate such a test we have calibrated the numbers of polar faculae in terms of magnetic flux normal to the solar surface, and we have measured fluxes associated with sunspot groups. We now turn our attention to these calibrations and measurements.

Second, we have calibrated the numbers of polar faculae in terms of magnetic flux normal to the solar surface and have found

that during the period 1905-1964 the polar flux maxima vary from
6 SFU to 21 SFU with 12 SFU being a typical maximum polar flux.
Our calibration is based on assigning 0. 2 SFU to a typical polar
facula. This value was obtained by averaging several flux measure-
ments (see Table 6) of equatorial faculae having size and intensity
similar to that of polar faculae. Although it is difficult to estimate
the accuracy of this 0. 2 SFU value, it would not be surprising if the
combined error due to both flux measurement and the selecting of
faculae were as much as ±0. 1 SFU. That is, we cannot expect the
figures 6 SFU, 21 SFU, and the typical 12 SFU above to be more
accurate than about ± 50%. Let us compare these results with the
Babcocks' (24) measured polar fluxes. They estimate that during
1953-54 the polar fluxes were roughly 8 SFU. Referring to
Figure 3 of Appendix III we find about 45 visible polar faculae for
each polar region in 1954. This corresponds to
1. 5 x 0. 2 SFU x 45 ~ 14 SFU for each entire polar region in 1954.

  Before leaving the topic of the polar fields, we shall consider
some observations that may help to clarify our ideas about the
polar fields and their relation to magnetic fields in the sunspot
belts. First, in the process of counting polar faculae several
plates were encountered on which the polar faculae were not centered
about the polemarker (see Figure 16(c)). In every such case, the
polemarker was found to be improperly placed, the correct position
always being midst the polar faculae. This shows that the polar
faculae are indeed polar phenomena and not just the trailing end of
unipolar magnetic regions that are expanding toward the poles.
Second, also in the process of counting polar faculae, large trailing
regions of equatorial faculae were observed streaming poleward and
eastward just prior to or during sunspot maximum in every sunspot

cycle during the period 1905-1964. These "streams", as they were called, undoubtedly correspond to the large UMRs described by Howard and Bumba (25). The streams were especially noticeable in the hemisphere whose pole was tipped away from the Earth. (This was because the tail ends of the streams in this hemisphere were 7° closer to the polar limb, whereas the tail ends of the streams in the other hemisphere were 7° farthur from the polar limb.) They extended to the polar regions, often coming within 30° of the poles themselves. (This includes the correction of 7° for the inclination of the sun's axis to the ecliptic.). Yet, during these times the immediate vicinity of the poles had very few if any polar faculae. Comparison of these white light photographs with polar magnetograms taken by Babcock during 1958 showed that these facula streams generally corresponded to magnetic fields having the polarity of the following sunspots of the corresponding hemisphere. These observations show that considerable care is necessary in the interpretation of polar magnetograms near the time of sunspot maximum because the facula streams could easily be mistaken for part of the polar fields. This is especially important in the hemisphere whose pole is tilted away from the Earth since the facula streams appear to extend nearly to the pole in that hemisphere. In summary then, these observations suggest that just prior to or during the time of sunspot maximum in every cycle considerable amounts of magnetic flux from the sunspot belts begin to arrive in the polar regions in great trailing streams. If we suppose (as was generally true during the last sunspot maximum) that these streams have predominantly the magnetic polarity of the following sunspots of the corresponding hemisphere, then we can account for the cancellation in the initial polar fields during or slightly after the

time of sunspot maximum in every cycle, and the buildup of new
polar fields shortly thereafter. Next we shall turn our attention
to magnetic field measurements in the sunspot belts.

Third, we know how much magnetic flux is provided by
sunspot groups as a function of their size, and, for two groups
relatively free from neighboring fields, we have seen how this
flux is distributed on the solar surface during the first few months
following their birth. Not only were the resulting field patterns of
these two groups roughly what one might expect from flux transport
by means of differential rotation plus a random-walk of step rate
corresponding to a ten year decay time of the polar field
(T_0 = 20 years in reference (2)), but also the fragmentary and
networklike concentrations of flux were what one might expect from
transport by means of the random-walk associated with the con-
vective supergranulation. This result encourages a further test
of the random-walk hypothesis. Since we now know the approximate
source fluxes of sunspot groups, we might hope to calculate the
collective effect of the many spot groups occurring during a sunspot
cycle. In this way we should expect to account for the formation of
the large UMRs that presumably correspond to the facula streams,
and to account for the detailed variation of the polar fields not only
within a sunspot cycle, but from cycle to cycle. Such a calculation
requires a knowledge not only of the source fluxes, but also of the
positions, the axial tilts, the doublet separations, and the times of
formation of the many individual sunspot groups occurring during a
sunspot cycle. Finally, note that if our flux measurements were all
inaccurate by a constant factor (for example, due to a calibration
error), this would only change our source flux spectrum $\Phi = 1.2 A_m$
by a constant factor which in turn would affect the calculated fields

by a constant factor. Since the polar fluxes themselves might be inaccurate by a constant factor due to the difficulty of calibrating the numbers of polar faculae, such errors would not seriously affect such a test of the random-walk hypothesis.

Fourth, we know that the source fluxes of BMRs are dispersed on the solar surface in progressively smaller bits and fragments of magnetic flux in which even the smallest features detectable by the photographic technique (roughly 1000 km in diameter) have fields of a few hundred gauss. In active regions we measured fields of as much as 700 gauss outside sunspots. Wherever we found fields of 800 gauss or more, we also found sunspots. We have already considered the accuracy of these field measurements in Parts II (D) and III (C). Although we cannot estimate the accuracy with certainty because of the unknown contrast during the projection printing stages of plate reduction, it seems unlikely that these measurements are inaccurate by more than a factor of two. Thus one could not interpret our measurements of 200-700 gauss outside sunspots to be less than 100-350 gauss. Next, we shall compare these results with the findings of other investigators.

Hale and his co-workers (26, 27) undertook a systematic search for "invisible" sunspots late in 1921 and early in 1922. By visually observing the separation of the components of a Zeeman-sensitive line, they obtained field strengths up to 700 gauss in active regions outside sunspots. Hale concluded that field strengths of 200-500 gauss in active regions were not uncommon outside sunspots. More recent photoelectric techniques at Mount Wilson have yielded fields generally in the range of 1-60 gauss in regions of Ca^+ K emission (23, 28, 29, 30). These fields are about a factor of ten smaller than our measurements, the discrepancy presumably

being due to both the superior seeing conditions and the superior spatial resolution achieved with our technique. In their early work, the Babcocks (24), using a slit 45 seconds of arc in length, noted calcium plages wherever the average field was 2 gauss or more. Howard (28) with an angular resolution of about 10 seconds of arc found that plages were outlined very nearly by a 10 gauss contour line. More recently, Howard and Harvey (30), with an angular resolution of 10 seconds of arc and with good seeing so that a resolution of 1 second of arc was realized, found that calcium plages were outlined by a 15 gauss contour. However, they suggested that if one considers that the magnetic gradient from a plage to non-plage region is probably not smooth and that the spatial resolution is only 10 seconds of arc, the actual field at the outer boundary of the plage is somewhat greater than 15 gauss, probably being 40-50 gauss. They stated further that the plages seen in the core of Hα fall within 60 gauss contour lines, although they do not entirely fill these lines. Since our measurements refer to the maximum field in small magnetic features, we should expect our field strengths to be somewhat greater than those of Howard and Harvey. Earlier, Howard (29), using an aperture of about 2 seconds of arc, measured r. m. s. magnetic field fluctuations of 8 gauss with peaks of 10-20 gauss spaced 20,000-30,000 km apart on the solar surface. He made these observations on six days between June 18 and July 17, 1959 in quiet regions away from plages. Our observations during the summer of 1964 showed that fields of 200 gauss occur in very small features less than 3000 km in diameter, and that these features correspond to brighter-than-average features in the core of Hα (see Figure 10). Since these bright features in Hα are distributed all over the solar surface, we might expect that

Howard would have encountered some. However, even if he had
encountered such a feature, seeing or guiding fluctuations might
have prevented its detection. Kiepenheuer (31) has shown the
importance of good seeing for magnetic field measurements at
the 150-foot tower at Mount Wilson. He used a photoelectric
instrument and a slit length corresponding to about 45,000 km
on the sun. During periods of good seeing, Kiepenheuer obtained
almost no field fluctuations from the slight displacement of the
solar image relative to the entrance slit when the image was out
of focus. When the image was in focus, a similar slight dis-
placement produced great fluctuations. On days of bad seeing,
he found large internal inconsistencies in his measurements.
Kiepenheuer concluded that the magnetic fields outside sunspot
groups have a fine structure whose dimension must be less than
about 10-20 seconds of arc, and that his measurements of a few
gauss represent averages of fields that might easily exceed
20 gauss even in quiet regions outside the sunspot belts. Beggs
and Von Klüber (32), using a magnetograph similar to that of the
Babcocks' (24), with a slit length of 4 seconds of arc found many
fields of strength up to 100 gauss outside spots in the sunspot belts.
They mention further that the sensitivity of their instrument is
limited by the seeing conditions. We might imagine that they
measured the relatively strong fields in plage regions and that with
better seeing they would have obtained field strengths somewhat
larger. Leighton (1), using the photographic technique, found fields
of 100-200 gauss in extensive areas throughout plage regions. In
summary, we note that as the sensitivity and resolution of magnetic
field measurements have improved, magnetic fields outside sunspots

have been found to occur in progressively smaller areas of
stronger field strength. We now observe fields of several
hundred gauss outside sunspots, just as Hale and co-workers
did in 1921-22 in their systematic search for "invisible" sunspots.

C. Conclusion

New measurements of solar magnetic fields have been
obtained. First, we have learned how much flux is associated
with sunspot groups of various sizes. Second, for two groups
relatively free from neighboring fields, we have seen how this
flux is distributed on the solar surface during the first few
months following their birth. Third, we have discovered how
strong the resulting magnetic fields are. Fourth, we have
determined the behavior of the polar fields over several solar
cycles. These measurements are generally consistent with the
hypothesis that bipolar magnetic regions are the sources of all
of the flux on the solar surface, and that the random-walk plus
differential rotation is the dominant mechanism for the distri-
bution of the flux provided by these sources. More important
than this however, these measurements provide a means of
testing this hypothesis in more detail than has heretofore been
possible. The logical consequence is to use these measurements
to calculate the cumulative effect of the many individual sunspot
groups that occur during a solar cycle. One might begin by
considering past sunspot cycles in order to test the hypothesis.
One would hope to account for the formation of the large unipolar
magnetic regions (facula streams) that expand poleward just prior
to or during sunspot maximum, as well as the detailed variation

of the polar fields themselves. If this were successful, one might use sunspot groups of the present cycle to predict the future polar fields. The chief difficulty would appear to be the measurement of the positions, the axial tilts, the doublet separations, and the dates of birth of the many individual sunspot groups during a solar cycle. This would be further complicated by the fact that many of the groups are born and die on the back side of the sun where they are not detected from the Earth. It is hoped that further study will yield a practical solution to this problem.

Appendix I.   Accuracy of the Approximation $4\gamma_M \delta = (\frac{\Delta T}{T})_{GM}$

In Part II of this thesis use was made of the fact that if $(\frac{\Delta T}{T})_{+}$ and $(\frac{\Delta T}{T})_{-}$ are the relative transmissions at the same solar position on each of a pair of Z-photos having reciprocal transmissions, then their geometrical mean, $(\frac{\Delta T}{T})_{GM}$, approximates $4\gamma_M \delta$ accurately for fields up to 1000 gauss.   This result will now be derived.

Let T_1 and T_2 be the transmissions on each of the two such Z-photos.   Then:

(1a) $$\frac{T_1}{T_{10}} = (\frac{1+\delta}{1-\delta})^{2\gamma_M}$$

(1b) $$\frac{T_2}{T_{20}} = (\frac{1-\delta}{1+\delta})^{2\gamma_M}.$$

Expanding these expressions in powers of δ, one obtains:

(2a) $$\frac{T_1}{T_{10}} = 1 + 4\gamma_M \delta \,[1 + E_1(\delta)\,]$$

(2b) $$\frac{T_2}{T_{20}} = 1 - 4\gamma_M \delta \,[1 - E_2(\delta)\,],$$

where $E_1(\delta)$ and $E_2(\delta)$ are the errors introduced by neglecting all the terms of order greater than first-order.   In particular,

(3a) $$E_1(\delta) = (\frac{1}{4\gamma_M \delta})[(\frac{1+\delta}{1-\delta})^{2\gamma_M} - (1 + 4\gamma_M \delta)\,]$$

(3b) $E_2(\delta) = (\frac{1}{4\gamma_M\delta})[(\frac{1-\delta}{1+\delta})^{2\gamma_M} - (1 - 4\gamma_M\delta)]$.

The relative transmissions, $(\frac{\Delta T}{T})_+$ and $(\frac{\Delta T}{T})_-$ are:

(4a) $(\frac{\Delta T}{T})_+ = 4\gamma_M\delta[1 + E_1(\delta)]$

(4b) $(\frac{\Delta T}{T})_- = -4\gamma_M\delta[1 - E_2(\delta)]$,

where $E_1(\delta)$ and $E_2(\delta)$ represent the errors in approximating $4\gamma_M\delta$ by $(\frac{\Delta T}{T})_+$ and $-(\frac{\Delta T}{T})_-$, respectively. The geometric mean, $(\frac{\Delta T}{T})_{GM}$, is then:

(5) $(\frac{\Delta T}{T})_{GM} = 4\gamma_M\delta \sqrt{[1 + E_1(\delta)][1 - E_2(\delta)]}$.

If one defines $\eta(\delta)$ by

(6) $1 + \eta(\delta) = \sqrt{[1 + E_1(\delta)][1 - E_2(\delta)]}$,

then

(7) $(\frac{\Delta T}{T})_{GM} = 4\gamma_M\delta[1 + \eta(\delta)]$.

Thus $\eta(\delta)$ is the accuracy of the approximation

(8) $(\frac{\Delta T}{T})_{GM} = 4\gamma_M\delta$.

For large fields, the errors $E_1(\delta)$ and $E_2(\delta)$ are relatively large, whereas the error $\eta(\delta)$ is relatively small. This can be seen best from power series expansions of these quantities:

(9a) $E_1(\delta) = a'\delta + b'\delta^2 + c'\delta^3 + d'\delta^4$

(9b) $E_2(\delta) = a'\delta - b'\delta^2 + c'\delta^3 - d'\delta^4$,

where:

$$a' = 2\gamma_M$$

$$b' = \frac{8\gamma_M^2 + 1}{3}$$

$$c' = \frac{4\gamma_M}{3}(2\gamma_M^2 + 1)$$

$$d' = \frac{32\gamma_M^4 + 40\gamma_M^2 + 3}{15} \quad .$$

An expansion of $\eta(\delta)$ then yields:

(10) $\eta(\delta) = p\delta^2 + q\delta^4$,

where $p = \dfrac{2\gamma_M^2 + 1}{3}$ and $q = \dfrac{2\gamma_M^4 + 10\gamma_M^2 + 3}{15} \quad .$

Note that $E_1(\delta)$ and $E_2(\delta)$ contain first- and third-order terms, whereas $\eta(\delta)$ does not. For a typical $\gamma_M \approx 3.0$ and $B_{||} \approx 1000$ gauss corresponding to $\delta \approx 0.1$, we have:

$$E_1(\delta) = 0.60 + 0.24 + 0.08 + 0.02 = 0.94$$

$$E_2(\delta) = 0.60 - 0.24 + 0.08 - 0.02 = 0.42 \quad ,$$

values that are neither equal nor small compared to unity, whereas $\eta(\delta) = 0.06 + 0.00 = 0.06$. Thus, for a line-of-sight component of magnetic field of 1000 gauss, the approximations $(\frac{\Delta T}{T})_+ = 4\gamma_M \delta$ and $(\frac{\Delta T}{T})_- = -4\gamma_M \delta$ are inaccurate by 94% and 42%, respectively, while the approximation $(\frac{\Delta T}{T})_{GM} = 4\gamma_M \delta$ is accurate within 6%.

Appendix II. Accuracy of the Approximation $\int_{A_0} (4\gamma_M{}^\delta)dA = (A_0 R)_{GM}$

In Part II use was made of the fact that if $A_0 R^+$ and $A_0 R^-$ are the quantities corresponding to the integrals of $(\frac{\Delta T}{T})_+$ and $(\frac{\Delta T}{T})_-$ respectively, then their geometric mean, $(A_0 R)_{GM}$, approximates $\int_{A_0} (4\gamma_M{}^\delta)dA$ accurately for magnetic fields up to 1000 gauss, and approximately for fields somewhat larger. This result will now be derived.

Using the terminology of Appendix I, we may write directly:

(1a) $A_0 R^+ = \int_{A_0} (4\gamma_M{}^\delta)[1 + E_1(\delta)]dA$

(1b) $-A_0 R^- = \int_{A_0} (4\gamma_M{}^\delta)[1 - E_2(\delta)]dA$.

The geometric mean of $A_0 R^+$ and $-A_0 R^-$ is then readily obtained:

$$(A_0 R)_{GM} = \int_{A_0} (4\gamma_M{}^\delta)dA \times$$

(2)
$$\sqrt{\left[1 + \frac{\int_{A_0} (4\gamma_M{}^\delta)E_1(\delta)dA}{\int_{A_0} (4\gamma_M{}^\delta)dA}\right]\left[1 - \frac{\int_{A_0} (4\gamma_M{}^\delta)E_2(\delta)dA}{\int_{A_0} (4\gamma_M{}^\delta)dA}\right]}$$

Next, defining the quantity ξ, by:

$$(3) \quad (1 + \xi)^2 = \left[1 + \frac{\int_{A_0} (4\gamma_M \delta) E_1(\delta) dA}{\int_{A_0} (4\gamma_M \delta) dA} \right] \left[1 - \frac{\int_{A_0} (4\gamma_M \delta) E_2(\delta) dA}{\int_{A_0} (4\gamma_M \delta) dA} \right] ,$$

one obtains the result:

$$(4) \quad (A_0 R)_{GM} = (1 + \xi) \cdot \int_{A_0} (4\gamma_M \delta) dA ,$$

where ξ is now the accuracy of the approximation:

$$(5) \quad (A_0 R)_{GM} = \int_{A_0} (4\gamma_M \delta) dA .$$

Using the series expansions for $E_1(\delta)$ and $E_2(\delta)$ given in equations (9a) and (9b) of Appendix I, one can estimate ξ from its definition (equation (3)):

$$(6) \quad \xi = b' \left\langle \delta^2 \right\rangle - \frac{(a')^2}{2} \left\langle \delta \right\rangle^2 \text{ to second-order terms,}$$

where a' and b' are the coefficients of the first two terms in the expansion of $E_1(\delta)$, and are given in Appendix I. The "averages",

$$\langle \delta \rangle = \frac{\int_{A_0} \delta^2 dA}{\int_{A_0} \delta dA} \quad \text{and} \quad \langle \delta^2 \rangle = \frac{\int_{A_0} \delta^3 dA}{\int_{A_0} \delta dA} \quad , \text{ are}$$

(automatically) performed over subregions of A_0 where the magnetic field is not zero. Just as we found from the expansion of η in Appendix I, first- and second-order terms in δ do not occur, and fourth-order terms are negligible for fields up to 1000 gauss.

We shall relate ξ to η by considering the fluctuations, $\Delta\delta$, of the magnetic field from its average:

(7) $\quad \Delta\delta = \delta - \langle \delta \rangle$.

Using this definition with the approximation for ξ (equation (6)), we find

(8) $\quad \xi = p \langle \delta \rangle^2 + b' \langle (\Delta\delta)^2 \rangle$,

where $p = b' - \frac{(a')^2}{2}$ is the same as the coefficient of δ^2 in the expansion for η given in Appendix I (equation (10)). Typically, $\gamma_M \approx 3.0$ so that $p \approx 6$ and $b' \approx 24$. We thus have:

(9a) $\quad \xi \approx 6 \langle \delta \rangle^2 + 24 \langle (\Delta\delta)^2 \rangle$

(9b) $\quad \eta(\delta) = 6\delta^2$.

Thus, if δ_0 corresponds to the largest line-of-sight component of magnetic field in the region of interest.

$$(10) \quad \frac{\xi}{\eta(\delta_0)} = \frac{\langle \delta \rangle^2 + 4 \langle (\Delta\delta)^2 \rangle}{\delta_0^2} \quad .$$

Typically, $\xi/\eta(\delta_0)$ ranges from approximately 0.4 for a field distribution that decreases linearly from the maximum δ_0 to 1.0 for a distribution that is uniform in the field regions and zero otherwise. In general, therefore, one would expect the approximation $(A_0 R)_{GM} = \int_{A_0} (4\gamma_M \delta) dA$ to be at least as accurate as the corresponding approximation $(\frac{\Delta T}{T})_{GM} = 4\gamma_M \delta$ applied to the largest field in the integration region A_0.

Appendix III

POLAR FACULAE DURING THE SUNSPOT CYCLE

NEIL R. SHEELEY, JR.

Norman Bridge Laboratory of Physics
California Institute of Technology
Received March 16, 1964

ABSTRACT

The numbers of north and south polar faculae have been counted for the period 1935–1963. The chief result is a variation of the numbers of polar faculae with time, approximately 180° out of phase with the time variation of the sunspot number for the whole solar disk. If the number of polar faculae and sunspot number both are plotted versus time with "polarities," the important feature appears that the numbers of polar faculae lag behind the sunspot number by approximately 90°. This is consistent with the supposition (Leighton 1963, 1964) that the sunspots provide a source of magnetic flux which is carried to the poles in a few years' time by means of a random-walk process associated with the convective supergranulation (Leighton, Noyes, and Simon 1962; Simon 1963). Comparison between the numbers of polar faculae and measurements of the polar magnetic field since 1952 (Babcock 1961; Howard 1963) suggests that the past observations of polar faculae can be used to extend measurements of polar magnetic field prior to 1952.

Polar faculae are visible on photographic plates taken daily in integrated sunlight using the 17-cm image at the 60-foot solar tower telescope of the Mount Wilson Observatory. The numbers of north and south polar faculae for the period 1935–1963 were obtained from these plates as follows:

First, for each year during 1935–1963, two 1-month time intervals were selected: February 15–March 15 and August 15–September 15. During the February 15–March 15 interval, the Earth has its southernmost heliographic latitude, so that the number of south polar faculae appearing on plates taken during this interval represents the true number of south polar faculae better than the number appearing on plates taken during any other 1-month interval of the year. Similarly, the August 15–September 15 interval exhibits the north polar cap best.

Second, for each interval the five plates of best seeing and contrast were selected subject to the condition that they had been exposed several days apart.

Third, two collections were formed, each containing approximately 150 plates. One collection, called the north deck, consisted of a set of the five plates from the August 15–September 15 interval for each year in the period 1935–1963. The other collection, the south deck, consisted of a set of the five plates from the February 15–March 15 interval for each year in the period 1935–1962. (No direct photographs were taken during the February 15–March 15, 1963, interval because the camera was being modified. Spectroheliograms taken at λ 6590 during this interval were meant to supplement the direct photographs, but they were not of sufficient quality for counting polar faculae.)

Fourth, the north and south decks were examined separately. The plates of the north deck were arranged in random order by a thorough shuffling. Next the number of north polar faculae on each plate was counted and recorded with the corresponding date of exposure. (The exposure date of each plate was not seen until after the number of faculae had been counted.) Then the list of numbers of north polar faculae and corresponding exposure dates was rearranged into chronological order. The number of north polar faculae for each year was obtained by averaging the five numbers obtained from the five plates of that year, and the corresponding root-mean-square deviation from this average was calculated. To obtain the number of south polar faculae for each year, a similar procedure was followed using the south deck.

Fifth, to test the consistency of this method, the north deck was reshuffled, and the entire process of counting, recording, unshuffling, averaging, and finding root-mean-

square deviations was repeated. Figure 1 shows the number of north polar faculae plotted versus time in years for both the original and repeated measurements. Because of the excellent agreement shown in Figure 1, the measurements of the south deck were not repeated.

Figure 2 shows the numbers of north and south polar faculae plotted versus time in years together with the Zürich mean daily sunspot relative number for the whole solar disk. Two features are apparent: (1) Since 1935 there has been a cyclic variation of both north and south polar faculae with time, about 180° out of phase with the variation of the sunspot number with time. (2) The behavior of the numbers of north and south polar faculae since the last sunspot maximum around 1958 deviates from this general pattern.

The existence of a strong spatial correlation between the line-of-sight component of photospheric magnetic field and the intensity of solar faculae (Leighton 1959; Simon 1963) suggests that polar faculae are a measure of the polar magnetic fields. This suggestion is strengthened further by magnetic field measurements obtained since 1952. Babcock (1961) reports that a general dipolar field existed at the time of the last sunspot minimum, that this field weakened and then underwent a reversal of magnetic polarity, first in the south and over a year later in the north. Figure 2 shows that the relatively large numbers of polar faculae occurring about the time of the last sunspot minimum decreased to relatively few at the time of sunspot maximum, after which the polar faculae appeared again in relatively large numbers, first in the south and about a year later in the north. Howard (1963) reports that in 1960 the south polar field weakened again, becoming zero around March, 1961. The north polar field had not significantly decreased. Figure 2 shows that the number of south polar faculae was less in 1960 than in 1959, and that it became quite small in 1961. The number of north polar faculae was relatively large in 1960 and even larger in 1961.

The fact that there have been essentially no polar faculae during each of the three past sunspot maxima, as shown in Figure 2, lends support to the supposition by Babcock (1961) that the reversal of the polar magnetic field of the Sun during the 1957–1958 sunspot maximum was not an isolated event, but the manifestation of a phenomenon which occurs about the time of solar maximum in every cycle. On this supposition one may wish to assign a "polarity" to the numbers of north and south polar faculae as shown in Figure 3 in order to facilitate their interpretation as a measure of the polar magnetic fields.[1] A "positive" number of polar faculae represents a positive magnetic field (magnetic vector directed toward the observer); a "negative" number of polar faculae represents a negative magnetic field. The assignment of facular "polarity" for the years since 1952 was made by comparison with the known polar field measurements (Babcock 1961; Howard 1963). The assignment was extended prior to 1952 by reversing the "polarity" at the time of polar facula minimum in each cycle. Also in Figure 3, the sunspot number has been plotted versus time with a "polarity." Although the sunspot number is for the whole solar disk, to show the comparison with the number of north and south polar faculae, respectively, the sunspot number has been assigned the polarity of the magnetic field of the following spots of the northern and southern hemispheres, respectively. (It seems preferable to compare the numbers of north and south polar faculae, respectively, with the sunspot numbers for the separate hemispheres. Current work to do this is in progress.) Figure 3 shows that the numbers of north and south polar faculae lag behind the sunspot number by approximately 90°.

Leighton (1963, 1964) has described a mechanism by which magnetic fields may be transported on the surface of the Sun. This mechanism is a random-walk process associated with a non-stationary large-scale cellular convection called "supergranulation" (Leighton, Noyes, and Simon 1962; Leighton and Simon 1963; Simon 1963). If a sunspot is regarded as the source of magnetic flux, the solar differential rotation will cause

[1] Since the writing of this paper, the author has extended the results of counting the polar faculae back to 1905, so they are included here in Figure 3.

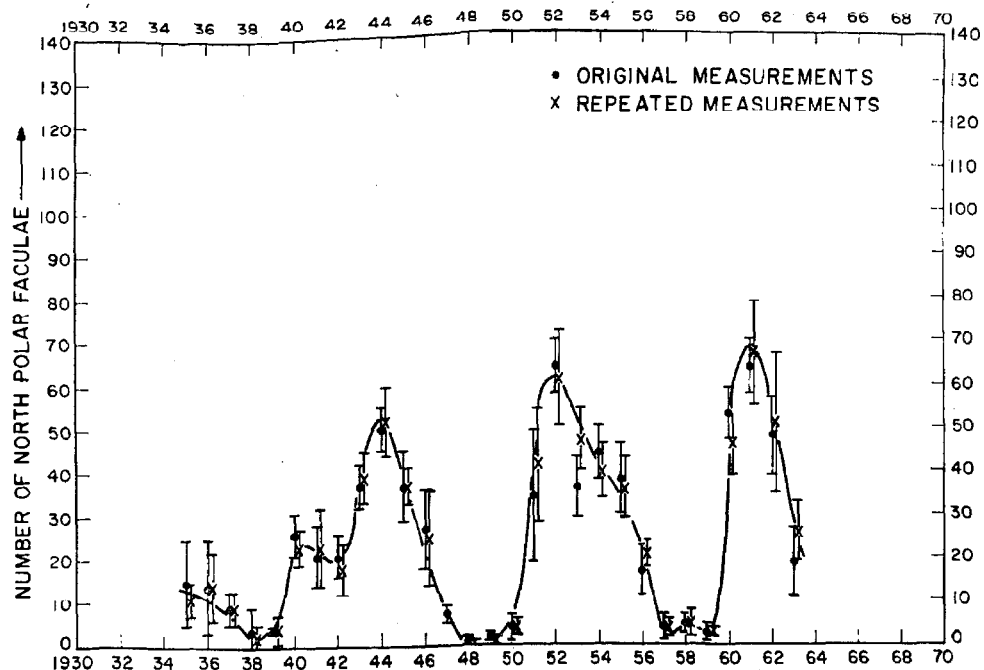* The result of this work is shown in Figure 17.

FIG. 1.—Number of north polar faculae versus time in years, illustrating the consistency of the method of measurement. The dots represent the first measurements obtained; the crosses represent repeated measurements of the same data. The crosses have been shifted slightly along the time axis for the sake of clarity. Each error bar has a full length of two root-mean-square deviations. The smooth curve has been drawn by eye.
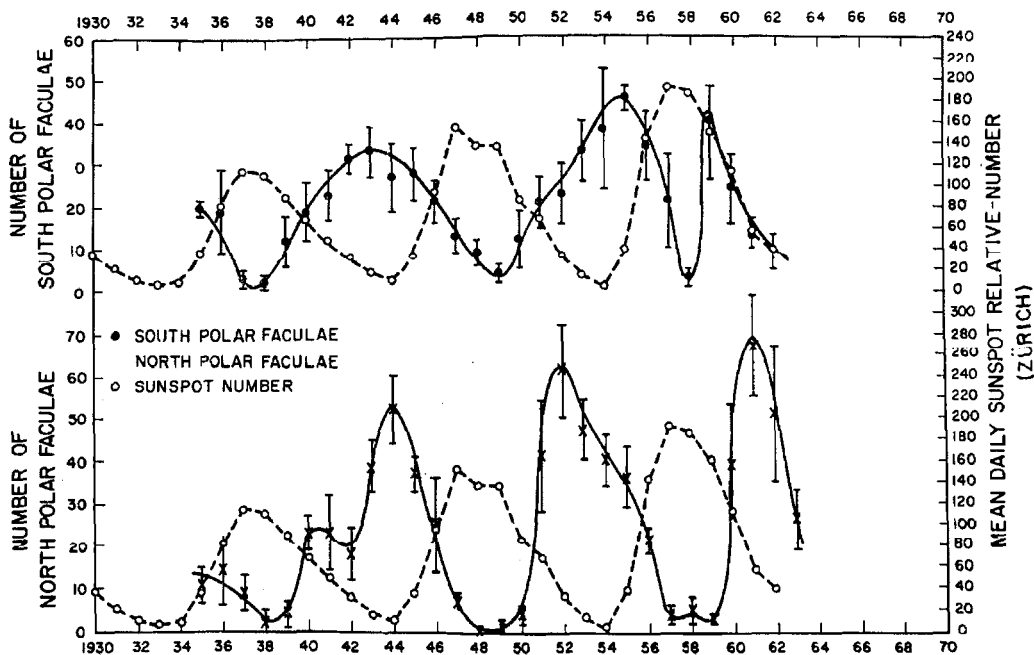

FIG. 2.—Comparison between the numbers of north and soth polar faculae, respectively, and the sunspot number for the whole solar disk. The upper and lower curves show the number of south and north polar faculae, respectively, with the numbers plotted on the left. The dotted lines show the sunspot number for the whole solar disk with the numbers plotted on the right. The smooth curves are drawn by eye.

this flux to be distributed in longitude, but not latitude. The random walk provides a component of motion in latitude as well as longitude. Since sunspots occur in groups of bipolar magnetic polarity in which the following part in each hemisphere is closer to the pole of that hemisphere than the preceding part (Babcock 1961; Brunner 1930), the net magnetic field that is transported to each pole has the sign of the magnetic field of the following spots of that hemisphere. Further, since the magnetic polarities of the following spots of one hemisphere are opposite to the magnetic polarities of the following spots of the other hemisphere, and since these magnetic polarities reverse with each new 11-year sunspot cycle, the net magnetic fields carried to the north and south poles, respectively, by the random walk have opposite polarities and reverse their polarities with each new 11-year sunspot cycle. The random walk occurs at a rate such that at a pole the effect of a source in the corresponding sunspot belt will be greatest from 1 to 4 years after the appearance of the source. Thus, the sunspots of each new cycle provide a
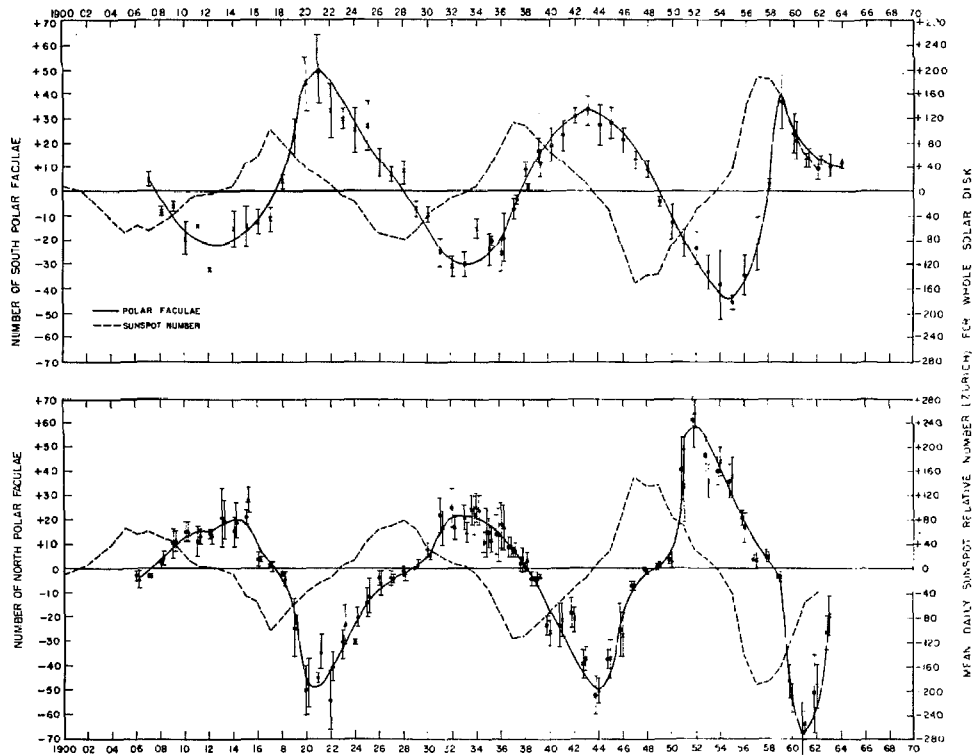

Fig. 3.—The numbers of north and south polar faculae versus time, plotted with "polarities" to represent polarities of the corresponding polar magnetic fields. A "positive" number of polar faculae represents a positive magnetic field (magnetic vector directed toward the observer), and a "negative" number represents a negative magnetic field (magnetic vector directed away from the observer). Solid curves are for numbers of faculae; dashed curves are for sunspot numbers. The solid curves have been drawn by eye. For some years, measurements of numbers of polar faculae have been repeated as indicated by more than one point for a given year. Not many data were available during February 15–March 15 for 1911, 1912, and 1913 as shown in the curve for the south polar faculae. The sunspot number for the whole solar disk is plotted twice with "polarities" for comparison with the numbers of north and south polar faculae. In each case, the "polarity" is the polarity of the magnetic fields of the following sunspots in the respective hemisphere.

source of magnetic flux which, during the first few years of the cycle, moves to the poles and begins to cancel the initial polar fields. About the time of sunspot maximum, sufficient magnetic flux has been transported to the poles to completely cancel the initial polar fields. In the next few years after the time of sunspot maximum, new polar fields are formed with polarities opposite both to the polarities of the corresponding old polar fields and to each other. The initial polarities are restored after another 11-year cycle. This entire process results in a time lag of the variation of the north and south polar magnetic fields behind sunspot activity by an amount depending on how much magnetic flux is released during a particular 11-year cycle, and on the rate at which this flux is released during that cycle. Thus, one would expect the behavior of the numbers of polar faculae since 1958 to be a direct consequence of the particular nature of the sunspot activity during the 1954-1964 cycle.

The polar faculae have been studied by Waldmeier (1962) and, since 1951, by Saito and Tanaka (1960). Waldmeier found that before 1951, polar faculae were rare, sporadic, and bore no relation to the sunspot cycle, in disagreement with the findings reported here. However, both Waldmeier and Saito and Tanaka found the general result that since 1951 there has been a variation of the numbers of polar faculae with time, approximately 180° out of phase with the time variation of the sunspot number for the whole disk. Waldmeier's observations since the last sunspot maximum are in excellent qualitative agreement with the findings reported here. He reports: "During the last sunspot maximum there were few polar faculae. In 1959 polar faculae appeared on the south polar cap. In 1960 they appeared at the north polar cap. In 1961 the south polar faculae were rare while the number of north polar faculae was greater than in 1960. In 1962 south polar faculae remained rare while the number of north polar faculae decreased to one-half of its 1961 value."

The results of Saito and Tanaka do not show detailed qualitative agreement during the period August 1951–June 1960. Any agreement between the results of Waldmeier, the results of Saito and Tanaka, and the results presented here may be fortuitous, since different methods of measurement were used in each case. For this reason, no quantitative comparison has been attempted.

Work is now under way to extend measurements of the number of north and south polar faculae back to 1905.[2]

REFERENCES

Babcock, H. W. 1961, *Ap. J.*, 133, 572.
Brunner, W. 1930, *Astr. Mitt. Zürich*, No. 124, p. 67.
Howard, R. F. 1963, *I.A.U. Symposium XXII, Conference on Stellar Magnetic Fields* (Tegensee, Germany).
Leighton, R. B. 1959, *Ap. J.*, 130, 366.
————. 1963, *I.A.U. Symposium XXII, Conference on Stellar Magnetic Fields* (Tegensee, Germany).
————. 1964, *Ap. J.* (in press).
Leighton, R. B., Noyes, R. W., and Simon, G. W. 1962, *Ap. J.*, 135, 474.
Leighton, R. B., and Simon, G. W. 1963, *A.J.*, 68, 291.
Saito, K., and Tanaka, Y. 1960, *Pub. Astr. Soc. Japan*, Vol. 12, No. 4.
Simon, G. W. 1963, Ph.D. thesis, California Institute of Technology.
Waldmeier, M. 1962, *Zs. f. Ap.*, 54, 260–267.

[2] See n. 1.

Figure 17

Monthly averages of the sunspot numbers, for the northern and southern hemispheres, derived from Fraunhofer Institut daily maps of the sun during the period 1956-1964. R_N and R_S refer to the sunspot numbers for the northern and southern hemispheres respectively. The g's refer to the number of groups and the f's refer to the number of spots.
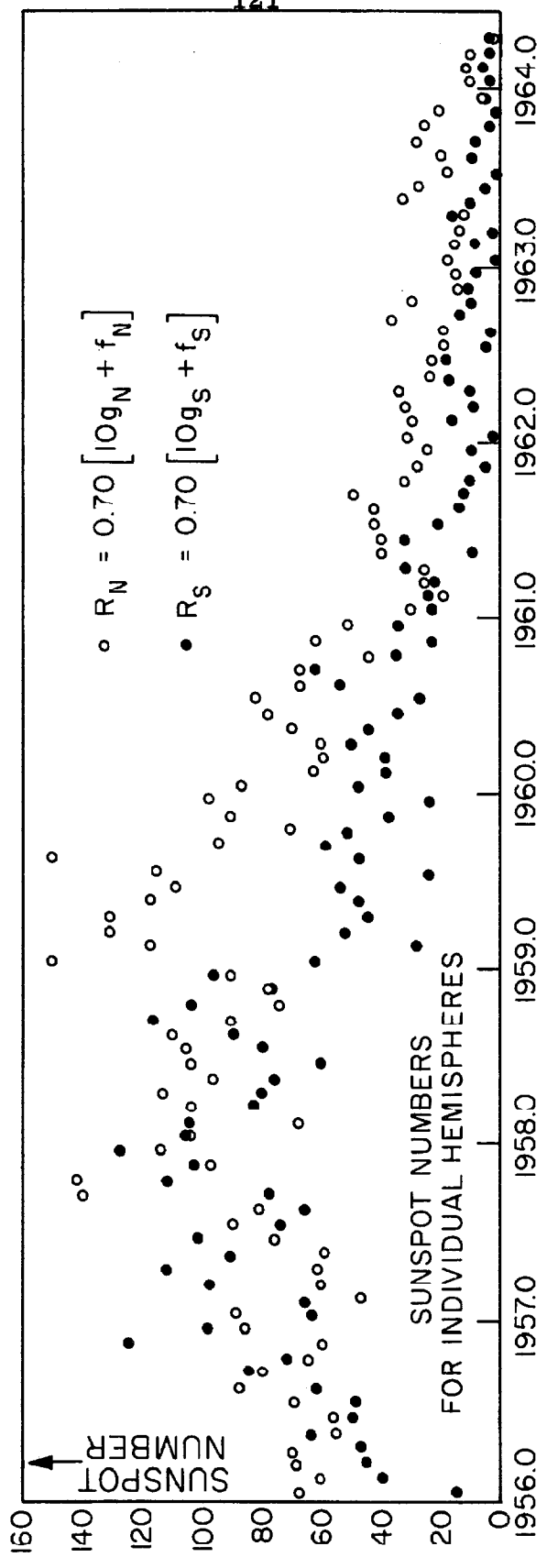
Figure 17

References

1. Leighton, R. B., Ap. J., 130, 366-380 (1959).

2. Leighton, R. B., Ap. J., 140, 1547 (1964).

3. Sheeley, Jr., N. R., Ap. J., 140, 731-735 (1964).

4. Leighton, R. B., I. A. U. Symposium XXII, Conference on Stellar Magnetic Fields (Tegensee, Germany, 1963).

5. Babcock, H. W., Ap. J., 118, 387-396 (1953).

6. Babcock, H. W., Ap. J., 133, 572-587 (1961).

7. Hale, G. E., Ap. J., 38, 27 (1913).

8. Hale, G. E. and Nicholson, S. B., Magnetic Observations of Sunspots (Carnegie Institution of Washington Publications, No. 498, 1938).

9. Leighton, R. B., Noyes, R. W., Simon, G. W., Ap. J., 135, 474-499 (1962).

10. Simon, G. W., Ph. D. Thesis, California Institute of Technology, 1963.

11. Brunner, W., Astr. Mitt. Zürich, No. 124, 67 (1930).

12. Howard, R. F., private communication, April 1963.

13. Cragg, T., Howard, R. F., Zirin, H., Ap. J., 138, 303 (1963).

14. St. John, C. E., et al., Revision of Rowland's Preliminary Table of Solar Spectrum Wave-Lengths with an Extension to the Present Limit of the Infra-Red, (Carnegie Institution of Washington Publications, No. 396, 1928).

15. Bumba, V., Bull. Astron. Inst. of Czech., 12, 82-92 (1961).

16. Houtgast, J., and Van Sluiters, A., Bull. Astron. Inst. Netherl., 10, 325 (1948).

17. de Jager, C., Handbuch d. Physik, 52, 154 (Berlin, Springer-Verlag, 1959).

18. Mattig, W., Z. Astrophys., 31, 273 (1953).

19. Cragg, T. and Utter, M. G., private communications, September 1964.

20. Wolfer, A., Pub. Zürich Obs., Vol. 2 (1899).

21. Losh, H. M., Pub. Obs. U. Michigan, 7, 127 (1939).

22. Roberts, P. H., private communication, December 1964.

23. Babcock, H. W., Ann. Rev. Astron. and Astrophys., 1, 41 (Annual Reviews, Inc., Palo Alto, 1963).

24. Babcock, H. D. and Babcock, H. W., Ap. J., 121, 349-366 (1955).

25. Howard, R. F. and Bumba, V., Ap. J., (to be published).

26. Hale, G. E., Pub. A. S. P., 34, 59 (1922).

27. Hale, G. E. and Nicholson, S. B., Magnetic Observations of Sunspots, Vol. 2, 576-580 (Carnegie Institution of Washington Publications, No. 498, 1938).

28. Howard, R., Ap. J., 130, 193-201 (1959).

29. Howard, R., Ap. J., 136, 211-222 (1962).

30. Howard, R. and Harvey, J. W., Ap. J., 139, 1328-1335 (1964).

31. Kiepenheuer, K. O., Ap. J., 117, 447 (1953).

32. Beggs, D. W. and Von Klüber, H., Nature, Lond., 178, 1412 (1956).